

From non-Hermitian linear response to dynamical correlations and fluctuation–dissipation relations in quantum many-body systems

Kevin T. Geier^{1,2,3,*} and Philipp Hauke^{1,2,3}

¹*INO-CNR BEC Center and Dipartimento di Fisica, Università di Trento, 38123 Povo, Italy*

²*Institute for Theoretical Physics, Ruprecht-Karls-Universität Heidelberg, Philosophenweg 16, 69120 Heidelberg, Germany*

³*Kirchhoff Institute for Physics, Ruprecht-Karls-Universität Heidelberg, Im Neuenheimer Feld 227, 69120 Heidelberg, Germany*

(Dated: April 12, 2021)

Quantum many-body systems are characterized by their correlations. While equal-time correlators and unequal-time commutators between operators are standard observables, the direct access to unequal-time *anti-commutators* poses a formidable experimental challenge. Here, we propose a general technique for measuring unequal-time anti-commutators using the linear response of a system to a non-Hermitian perturbation. We illustrate the protocol at the example of a Bose–Hubbard model, where the approach to thermal equilibrium in a closed quantum system can be tracked by measuring both sides of the fluctuation–dissipation relation. We relate the scheme to the quantum Zeno effect and weak measurements, and illustrate possible implementations at the example of a cold-atom system. Our proposal provides a way of characterizing dynamical correlations in quantum many-body systems with potential applications in understanding strongly correlated matter as well as for novel quantum technologies.

I. INTRODUCTION

Many fundamental properties of quantum many-body systems are encoded in their dynamical correlations, involving observables at unequal times. They are at the basis of ubiquitous phenomena ranging from optical coherence [1, 2] and transport phenomena [3, 4], over far-from-equilibrium universality [5–8], glassy dynamics and aging [9–11], as well as dynamical topological transitions [12], to thermalization, integrability, and quantum chaos [13–17]. Historically, a groundbreaking role has been played by the fluctuation–dissipation relation (FDR) [18–20], which can be viewed as a generalization of the famous Einstein relation for Brownian motion [21]. In essence, the FDR connects unequal-time commutators and anti-commutators: in thermal equilibrium, fluctuations of an observable at any given frequency are intrinsically connected with the energy dissipated when the system is perturbed at that same frequency. As it is governed by a single global parameter, the temperature, the FDR is an excellent probe for thermalization of closed quantum systems [22–26]. Certifying that a given quantum state is thermal can be valuable, e.g., for applying dynamical protocols to detect entanglement [27, 28] — a key resource for quantum-enhanced metrology [29, 30].

Notwithstanding its fundamental importance, both sides of the FDR have thus far only been measured for classical systems [31–33]. For quantum systems, only one side, the unequal-time commutator, is easily accessible thanks to Kubo’s celebrated linear-response theory [4, 20]. A main difficulty stems from the fact that a projective von Neumann measurement at a particular time collapses the quantum state [34], hindering a mea-

surement of the time–time correlation with respect to the initial state. Despite several proposals for measuring unequal-time correlations on various platforms [26, 35–42], as of today, an experimental observation of the unequal-time anti-commutator in a quantum many-body system remains elusive.

Here, we discuss how a linear response to a non-Hermitian perturbation [43, 44] permits direct experimental observation of the unequal-time anti-commutator. Combined with a traditional method for measuring the corresponding unequal-time commutator, e.g., standard linear response, this scheme gives access to both sides of the FDR independently, allowing one to track a system’s evolution towards thermal equilibrium. We illustrate this possibility by means of numerical simulations at an example motivated by a ground-breaking cold-atom experiment [45] — a Bose–Hubbard system that is quenched from a Mott-insulating initial state to the superfluid phase (see Fig. 1).

The key to measuring unequal-time anti-commutators is the ability to engineer (effective) non-Hermitian perturbations. In recent years, a tremendous interest in non-Hermitian physics has emerged [46, 47], stimulated by the rapid progress in the experimental generation and control of non-Hermitian systems [48–53]. Indeed, non-Hermiticity gives rise to a wealth of new physics with novel (topological) phases and unconventional critical behavior [54–59], bearing a vast potential for applications, e.g., in strongly enhanced quantum sensing [60, 61] or adiabatic quantum optimization [62, 63]. Leveraging on this development, we design a specific protocol to generate effective non-Hermitian dynamics in a system of cold atoms, enabling access to the left-hand side of the FDR. Our scheme is most conveniently phrased as an application of the quantum Zeno effect [64, 65], combining outcoupling to an ancillary system with a projection on the Zeno subspace given by the empty ancilla. In a

* kevinthomas.geier@unitn.it

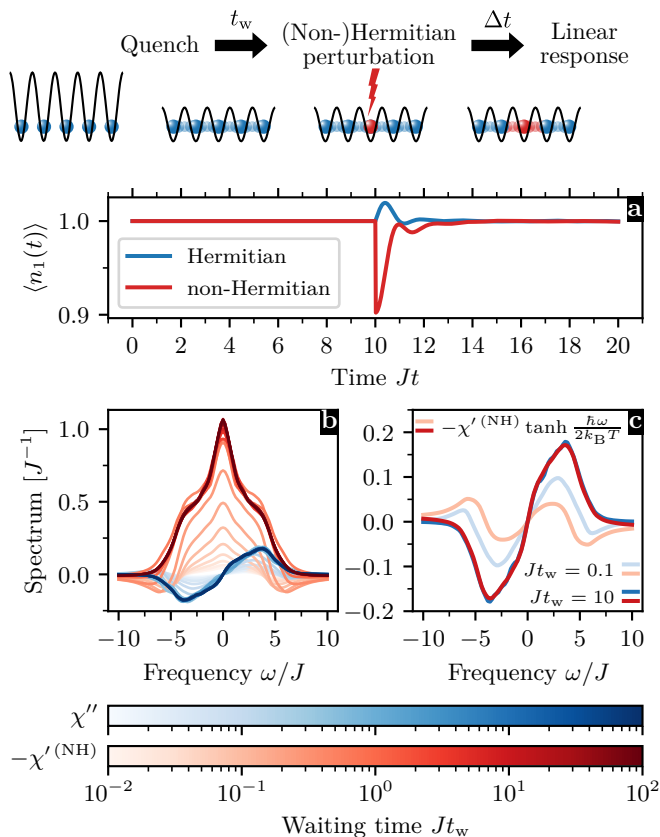


Figure 1. (Non-)Hermitian linear response protocol for measuring fluctuation–dissipation relations (FDRs), exemplified for a Bose–Hubbard chain. (a) Schematic illustration of the protocol and response of the density $\langle n_1(t) \rangle$ to an (anti-)Hermitian perturbation $H_1 = -(i)\hbar s \delta(t-t_w) n_1$ of strength $s = 0.05$, applied at the waiting time $Jt_w = 10$. (b) Thermalization dynamics of the dissipative part of the “Hermitian” dynamic susceptibility $\chi''_{n_1 n_1}(t_w, \omega)$ (“commutator”) and the reactive part of the “non-Hermitian” dynamic susceptibility $\chi'_{n_1 n_1}^{(NH)}(t_w, \omega)$ (“anti-commutator”). (c) $\chi'_{n_1 n_1}^{(NH)}$ rescaled by $-\tanh(\hbar\omega/2k_B T)$ in comparison with $\chi''_{n_1 n_1}$. The effective temperature T is determined according to Eq. (16) as the best value of T (in a least squares sense) that relates these two susceptibilities via the FDR (13), yielding $k_B T/\hbar J = \{4.5, 4.2\}$ for $Jt_w = \{0.1, 10\}$, respectively. The FDR is clearly violated at early times, but it is restored at late times when the system has thermalized.

cold-atom implementation, this can be realized through a coherent or dissipative perturbation in the linear regime, together with the ability of distinguishing zero from non-vanishing ancilla population in post-selection. Two variants of our scheme are presented, the first one corresponding to a measurement of unequal-time correlations in time domain and the second one harnessing engineered dissipation [66, 67] to realize a measurement of dynamic susceptibilities in frequency domain. To demonstrate the feasibility of our proposal, we discuss experimental error sources and we benchmark both protocols by numerically solving the full quantum evolution, including the

stochastic dynamics underlying the dissipative scheme. We also discuss formal relations to the framework of weak measurements (see Ref. [68] for a comprehensive review) and the paradigm of generating non-Hermitian dynamics in dissipative quantum systems by post-selecting individual quantum trajectories on the absence of quantum jumps [52, 59, 69–71]. Our approach opens the door to probing the FDR in quantum many-body systems in an unbiased way and for a broad range of observables.

II. THE FLUCTUATION–DISSIPATION RELATION

For a quantum many-body system in thermal equilibrium, the FDR [20] links the symmetrized correlation spectrum $S_{BA}(\omega)$ of any two operators A and B across the entire frequency spectrum ω to the dissipative part of the dynamic susceptibility $\chi''_{BA}(\omega)$ via

$$S_{BA}(\omega) = \hbar \coth\left(\frac{\hbar\omega}{2k_B T}\right) \chi''_{BA}(\omega), \quad (1)$$

where \hbar is the reduced Planck constant and k_B is the Boltzmann constant. This elegant relation requires only a single parameter as input, the global temperature T . The ease of accessing $\chi''_{BA}(\omega)$ can then be exploited to obtain $S_{BA}(\omega)$. However, when the system is far from equilibrium, the two sides of Eq. (1) become non-stationary and the FDR can be broken [25], making it necessary to devise independent handles on both sides of the relation.

One can generalize the definitions of S and χ'' to such a non-equilibrium situation by introducing the response function

$$\phi_{BA}(t, t') = \frac{i}{\hbar} \theta(t - t') \langle [B(t), A(t')] \rangle_0 \quad (2)$$

and the symmetrized dynamic correlation function

$$S_{BA}(t, t') = \frac{1}{2} \langle \{B(t), A(t')\} \rangle_0 - \langle B(t) \rangle_0 \langle A(t') \rangle_0, \quad (3)$$

defined, respectively, in terms of the unequal-time commutator and anti-commutator of the Heisenberg operators $A(t)$ and $B(t)$. Here, $\theta(t)$ is the Heaviside step function, ensuring causality of the response, and the subscript in the expectation value $\langle \dots \rangle_0$ signifies that the Heisenberg operators evolve under the (unperturbed) Hamiltonian H_0 . Equation (2) is the non-equilibrium version of Kubo’s well-known linear response function [20], which determines the evolution of the expectation value $\langle B(t) \rangle$ under the perturbed Hamiltonian $H(t) = H_0 + H_1(t)$, to linear order in the perturbation $H_1(t) = -f(t)A$, according to

$$\langle B(t) \rangle = \langle B(t) \rangle_0 + \int_0^t dt' \phi_{BA}(t, t') f(t'). \quad (4)$$

In contrast to the usual equilibrium linear response scenario, the initial state is not necessarily stationary with

respect to H_0 . In this situation, it is common to define the non-equilibrium generalization of the dynamic susceptibility χ as the Fourier transform of the response function ϕ with respect to the relative time $\Delta t = t - t'$ at fixed central time $\tau = (t + t')/2$ [72],

$$\chi_{BA}(\tau, \omega) = \int_{-2\tau}^{2\tau} d\Delta t \phi_{BA}\left(\tau + \frac{\Delta t}{2}, \tau - \frac{\Delta t}{2}\right) e^{i\omega\Delta t}. \quad (5)$$

This quantity is commonly decomposed as $\chi_{BA} = \chi'_{BA} + i\chi''_{BA}$ into a reactive part $\chi'_{BA}(\tau, \omega) = [\chi_{BA}(\tau, \omega) + \chi_{AB}(\tau, -\omega)]/2$ and a dissipative (or absorptive) part $\chi''_{BA}(\tau, \omega) = [\chi_{BA}(\tau, \omega) - \chi_{AB}(\tau, -\omega)]/2i$ (cf. Ref. [3]), the latter entering the right-hand side of the FDR (1). The correlation spectrum $S(\tau, \omega)$ on its left-hand side can be defined analogously to Eq. (5) as the Fourier transform of Eq. (3).

For a thermalizing system, we expect $\chi_{BA}(\tau \rightarrow \infty, \omega)$ and $S_{BA}(\tau \rightarrow \infty, \omega)$ to reach steady values that fulfill the FDR. As such, the restoration of the FDR provides an excellent probe for how and when a quantum many-body system approaches thermal equilibrium. While the commutator in Eq. (2) can be accessed rather straightforwardly, for example, by studying how energy is absorbed or how an observable deviates from its equilibrium value following a time-dependent perturbation [20], the determination of the unequal-time anti-commutator in Eq. (3) is, unfortunately, considerably more challenging. We now exploit an extension of the framework of linear response theory to non-Hermitian Hamiltonians [43, 44], giving access to the left-hand side of Eq. (1), and thus enabling direct probes of the FDR.

III. NON-HERMITIAN LINEAR RESPONSE THEORY

Though long established in the context of open quantum systems [73, 74], recent years have seen a surge of interest in quantum systems with non-Hermitian Hamiltonians [47]. Here, we tap into this development by exploiting the linear response to a non-Hermitian perturbation [43, 44] in order to extract unequal-time anti-commutators.

In contrast to usual linear response theory, we assume that the system is effectively described by a non-Hermitian Hamiltonian $H(t) = H_0 + H_1(t)$, where H_0 is the unperturbed (Hermitian) Hamiltonian and $H_1(t) = -if(t)A$ is an anti-Hermitian perturbation with a positive semi-definite operator A and a non-negative time-dependent function $f(t)$. For example, such a scenario arises in the quantum trajectories approach to dissipative quantum systems [69–71] if the evolution is conditioned on the absence of quantum jumps [50, 52, 59]. In Section V, we present a scheme for engineering effective non-Hermitian Hamiltonians specifically designed for measuring FDRs.

A quantum state described by the density operator $\rho(t)$ evolves in time under the non-Hermitian Hamil-

tonian $H(t)$ according to the von Neumann equation

$$i\hbar \frac{d}{dt} \rho = H(t)\rho - \rho H^\dagger(t) = [H_0, \rho] + \{H_1(t), \rho\} \quad (6)$$

with initial condition $\rho(0) = \rho_0$.

Using time-dependent perturbation theory, a straightforward calculation (reported in Appendix A) shows that, to linear order in the perturbation, the unnormalized expectation value of a (Hermitian) observable B is given by

$$\text{Tr } B\rho(t) = \langle B(t) \rangle_0 - \frac{1}{\hbar} \int_0^t dt' \langle \{B(t), A(t')\} \rangle_0 f(t'). \quad (7)$$

The non-Hermiticity of the perturbed Hamiltonian has the important consequence that the state $\rho(t)$ is no longer normalized: as can be seen by inserting the identity operator for B in Eq. (7), its norm decreases with time, to linear order, as

$$\text{Tr } \rho(t) = 1 - \frac{2}{\hbar} \int_0^t dt' \langle A(t') \rangle_0 f(t'). \quad (8)$$

Physically, this decrease can be interpreted as the leakage of the wave function into a complementary state space (see also Section V). To account for this loss of probability, we consider the normalized expectation value $\langle B(t) \rangle = \text{Tr}[B\rho(t)]/\text{Tr } \rho(t)$, describing a post-selected measurement [68]. Combining Eqs. (7) and (8), the disconnected correlations drop out to linear order, and we can write the response as

$$\langle B(t) \rangle = \langle B(t) \rangle_0 + \int_0^t dt' \phi_{BA}^{(\text{NH})}(t, t') f(t') \quad (9)$$

with the “non-Hermitian” response function

$$\phi_{BA}^{(\text{NH})}(t, t') = -\frac{1}{\hbar} \theta(t - t') \left[\langle \{\hat{B}(t), \hat{A}(t')\} \rangle_0 - 2 \langle \hat{B}(t) \rangle_0 \langle \hat{A}(t') \rangle_0 \right]. \quad (10)$$

Here, we have inserted the Heaviside step function θ to ensure causality of the response. Remarkably, the non-Hermitian response function in Eq. (10) is the desired measurable quantity that gives direct access to the unequal-time anti-commutator (3) by virtue of the relation $\phi_{BA}^{(\text{NH})}(t, t') = -2\theta(t - t')S_{BA}(t, t')/\hbar$.

To establish a link between the response function (10) and the correlation spectrum appearing on the left-hand side of the FDR (1), we define the “non-Hermitian” dynamic susceptibility, similarly to Eq. (5), as the Fourier transform

$$\chi_{BA}^{(\text{NH})}(\tau, \omega) = \int_{-2\tau}^{2\tau} d\Delta t \phi_{BA}^{(\text{NH})}\left(\tau + \frac{\Delta t}{2}, \tau - \frac{\Delta t}{2}\right) e^{i\omega\Delta t}. \quad (11)$$

We can split this quantity as $\chi_{BA}^{(\text{NH})} = \chi'_{BA}^{(\text{NH})} + i\chi''_{BA}^{(\text{NH})}$ into the components

$$\chi'_{BA}^{(\text{NH})}(\tau, \omega) = \frac{1}{2} \left[\chi_{BA}^{(\text{NH})}(\tau, \omega) + \chi_{AB}^{(\text{NH})}(\tau, -\omega) \right], \quad (12a)$$

$$\chi''_{BA}^{(\text{NH})}(\tau, \omega) = \frac{1}{2i} \left[\chi_{BA}^{(\text{NH})}(\tau, \omega) - \chi_{AB}^{(\text{NH})}(\tau, -\omega) \right], \quad (12b)$$

which we refer to, in analogy to their Hermitian counterparts, as the reactive and dissipative parts of the non-Hermitian susceptibility, respectively. As shown in Appendix A, the reactive part (12a) gives access to the correlation spectrum via the identity $S_{BA}(\tau, \omega) = -\hbar\chi'_{BA}{}^{(\text{NH})}(\tau, \omega)$. This allows us to rewrite the FDR (1) in thermal equilibrium as

$$\chi'_{BA}{}^{(\text{NH})}(\omega) = -\coth\left(\frac{\hbar\omega}{2k_{\text{B}}T}\right)\chi''_{BA}(\omega), \quad (13)$$

which is expressed entirely in terms of the susceptibilities $\chi'_{BA}{}^{(\text{NH})}$ and χ''_{BA} , accessible using non-Hermitian and standard (Hermitian) linear response, respectively. As such, linear response theory provides a framework for independently probing both sides of the FDR (13) out of equilibrium.

It is worthwhile emphasizing that the outlined derivation of the response to a non-Hermitian perturbation is by no means restricted to the linear regime only, but, as well-known in standard response theory [19], can be extended to non-linear responses. In fact, by calculating the linear approximations in Eqs. (7) and (8) to the desired non-linear order, one can in principle access an infinite hierarchy of unequal-time correlations, order by order.

IV. ILLUSTRATION: QUENCH IN A BOSE-HUBBARD SYSTEM

If a system of interest is coupled to a large thermal bath, it will sooner or later always approach thermal equilibrium with the bath temperature [74], and the FDR will eventually hold. In contrast, the question how and whether a closed quantum system thermalizes once it is brought out of equilibrium is much more subtle [13–17]. In ground-breaking cold-atom experiments, it has been shown that even in very small interacting quantum systems, expectation values can reach steady states that are consistent with thermal equilibrium [45]. We now illustrate how such an experiment could go one step further by demonstrating the validity of the FDR.

To this end, we numerically solve the full quantum evolution for the Bose–Hubbard chain describing the experiment in Ref. [45] (we emphasize that our approach does not depend on such a model choice and can be applied to general quantum systems). The system Hamiltonian is

$$H_0 = -\hbar J \sum_{\ell=1}^L (a_{\ell}^{\dagger} a_{\ell+1} + \text{h.c.}) + \frac{\hbar U}{2} \sum_{\ell=1}^L n_{\ell}(n_{\ell} - 1). \quad (14)$$

Here, the optical lattice sites are denoted by $\ell = 1 \dots L$ with associated bosonic annihilation, creation, and number (density) operators a_{ℓ} , a_{ℓ}^{\dagger} , and n_{ℓ} , respectively. J is the strength of the nearest-neighbor hopping, for which we assume periodic boundary conditions, and U the on-site interaction rate.

The linear response protocol is illustrated at the top of Fig. 1. We initialize the system of $N = L$ bosons in a Mott-insulating state at $J/U \rightarrow 0$ and then quench it at time $t = 0$ deeply into the superfluid phase at $J/U = 0.64^1$. This quench throws the system heavily out of equilibrium. After a variable waiting time t_{w} , we either apply a Hermitian or an anti-Hermitian perturbation in order to access the desired response functions in Eq. (2) or Eq. (10), respectively. The perturbation is applied as a rectangular pulse of strength s and duration δt , $f(t) = \hbar s [\theta(t - t_{\text{w}}) - \theta(t - t_{\text{w}} - \delta t)]/\delta t$. The exact shape of the pulse is unimportant as long as the pulse duration is sufficiently short compared to the characteristic time scales of the system (cf. Appendix B). In this case, the pulse can be approximated by a delta function as $f(t) \approx \hbar s \delta(t - t_{\text{w}})$. Figure 1a shows the time trace of the response to a (non-)Hermitian perturbation giving access to density autocorrelations ($B = A = n_1$) for a system of $L = 12$ sites.

The susceptibilities appearing in the FDR (13) can be found by varying both the waiting time t_{w} and the observation time $t = t_{\text{w}} + \Delta t$, and computing the Fourier transform with respect to the relative time Δt at fixed central time τ according to Eqs. (5) and (11). However, since at early times τ the integration domains of the Fourier integrals in Eqs. (5) and (11) are limited to only a short range of Δt , we consider instead the non-equilibrium generalization of the susceptibility as the Fourier transform of the response function at fixed waiting time t_{w} [25],

$$\chi_{BA}{}^{(\text{NH})}(t_{\text{w}}, \omega) = \int_{-\infty}^{\infty} d\Delta t \phi_{BA}{}^{(\text{NH})}(t_{\text{w}} + \Delta t, t_{\text{w}}) e^{i\omega\Delta t}, \quad (15)$$

and analogously for its Hermitian counterpart. This form has the advantage that the integration domain is unbounded, and it is often more efficient to compute as the integrand is directly obtained from the linear response at fixed waiting times. In practice, the integral in Eq. (15) needs to be regulated appropriately, for example, by truncating it once the correlations have decayed sufficiently or by means of a frequency filter accounting for a finite spectral resolution in experiments. For the purposes of this section, we follow the latter approach, using an exponential filter of characteristic frequency $\gamma/J = 0.2$, which amounts to the replacement $e^{i\omega\Delta t} \rightarrow e^{(i\omega - \gamma)\Delta t}$ in the Fourier integral (15). Note that out of equilibrium, the susceptibilities in Eqs. (11) and (15) generally disagree, and, in particular, $S_{BA}(t_{\text{w}}, \omega) \neq -\hbar\chi'_{BA}{}^{(\text{NH})}(t_{\text{w}}, \omega)$ in general (cf. Appendix A). Once the system has reached a stationary state, the response functions depend only on the relative time Δt and the different conventions become equivalent, provided the integration domains are chosen appropriately. Here, we probe the FDR out of equilibrium in the form of Eq. (13), expressed in terms of the

¹ The results are insensitive to the precise choice of parameters.

susceptibilities obtainable from the (non-)Hermitian linear response at fixed waiting time as in Eq. (15). Moreover, while in general the susceptibility components in Eq. (12) are complex [3] and require measurements of both the response of B to a perturbation by A and vice versa, for our model system and our choice of observables², these quantities are real and simply given, respectively, by the real and imaginary parts of the susceptibility (15) (and similarly for the Hermitian susceptibility in Eq. (5)).

Figure 1b shows the thermalization dynamics of $\chi'^{(\text{NH})}$ and χ'' for density autocorrelations ($B = A = n_1$) at different waiting times t_w , computed in a system of $L = 12$ sites for a perturbation of strength $s = 0.05$ and duration $J\delta t = 0.01$. $\chi'^{(\text{NH})}$ is symmetric in ω and grows as a broad central peak with small wings of opposite sign that gradually disappear as t_w increases, while χ'' is anti-symmetric and develops characteristic peaks around non-zero frequencies. To assess whether the two functions satisfy the FDR, we use the least squares method to find the effective temperature T that best relates the susceptibilities via the FDR (13), i.e., for a fixed waiting time t_w ,

$$T = \arg \min_{\Theta} \int d\omega \left[\chi'^{(\text{NH})} \tanh \frac{\hbar\omega}{2k_B\Theta} - (-\chi'') \right]^2. \quad (16)$$

In Fig. 1c, one can see that the FDR is clearly violated at early times, i.e., there exists no global value of T such that Eq. (13) holds, but at later times, the agreement is remarkable and supports the interpretation that the system undergoes thermalization.

A distinct feature of the FDR in equilibrium is that it holds for any pair of observables A and B . To confirm this prediction for our model system, we have computed $\chi'^{(\text{NH})}$ and χ'' for off-site density correlations corresponding to $A = n_1$ and $B = n_{1+d}$ as a function of the distance d . The results are shown in Fig. 2a, where $\chi'^{(\text{NH})}$ is rescaled according to Eq. (13) with the best-fitting effective temperature T obtained from Eq. (16) for each configuration (t_w, d). Qualitatively, it can be seen that the two quantities deviate for early times, but agree well for late times. To make this statement more quantitative, in Fig. 2c, we show the L^2 norm of the error $\|\chi'^{(\text{NH})} \tanh(\hbar\omega/2k_B T) - (-\chi'')\|$, normalized to the sum of the individual norms, which acts as a figure of merit measuring how well the FDR (13) is fulfilled at a particular instance of time. For small distances, the relative error becomes vanishingly small after waiting times

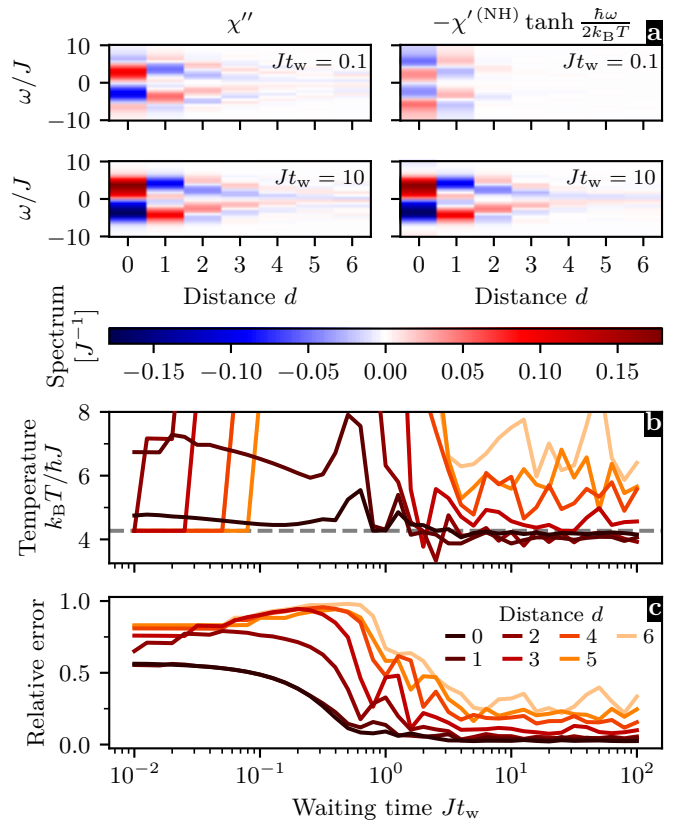


Figure 2. Thermalization dynamics of density correlations in a Bose-Hubbard system. (a) Comparison of $\chi''_{n_1 n_{1+d}}$ and $\chi'^{(\text{NH})}_{n_1 n_{1+d}}$, rescaled by $-\tanh(\hbar\omega/2k_B T)$, for different waiting times t_w as a function of the spatial distance d . The effective temperature T is determined for each configuration according to Eq. (16) using the least squares method. At early times, clear deviations are visible, but for late times and small distances, the two quantities agree and the FDR (13) is fulfilled. (b, c) Least squares value of the effective temperature T and relative error of the FDR as a function of the waiting time t_w for several distances d . At small distances, after times on the order of J^{-1} , the effective temperature approaches a constant value consistent with the prediction $\langle H_0 \rangle_T = E_0$ for a thermal state (grey dashed line), and the relative error becomes small. As the distance becomes comparable to the system size, the agreement becomes worse and the FDR is broken, reflecting the purity of the global quantum state.

on the order of J^{-1} , while for larger distances, the error tends to drop later and fluctuates around a non-zero offset. A similar behavior is exhibited by the effective temperature (see Fig. 2b): at small distances and late times, the temperatures are approximately constant and agree with each other, while this is no longer true for larger distances. The breaking of the FDR is expected when the considered distance becomes comparable to the size of the total system, since globally, the system remains in a pure state. The effective temperature at which the system thermalizes is consistent with the one obtained for a thermal state using the condition $\langle H_0 \rangle_T = E_0$ (grey dashed line at $k_B T / \hbar J = 4.27$ in Fig. 2b, calculated for

² Sufficient conditions for the reactive and dissipative parts of the dynamic susceptibility to be real include the case $B = A^\dagger$, or, if A and B are Hermitian, the property $\langle B(t)A(t') \rangle = \langle A(t)B(t') \rangle$. The latter is fulfilled, for instance, if A and B are on-site observables in a system that is invariant under both translations and reflections, as it is the case for density-density correlations in a Bose-Hubbard chain with periodic boundary conditions.

$L = 8$ using exact diagonalization), where $\langle \dots \rangle_T$ denotes the expectation value with respect to a canonical ensemble at temperature T , and E_0 is the energy of the initial state after the quench [45].

Having illustrated how the FDR becomes accessible via (non-)Hermitian linear response, we now turn to the question of how to realize the required non-Hermitian Hamiltonian experimentally.

V. REALIZATION OF A NON-HERMITIAN HAMILTONIAN

There exists a growing body of work that describes how non-Hermitian physics can be generated in quantum many-body systems [46, 47]. Non-Hermitian Hamiltonians naturally arise in the context of dissipative quantum systems [73, 74], where they govern the evolution of individual quantum trajectories conditioned on the absence of quantum jumps [69–71]. This way, it is possible to harness natural sources of dissipation in order to explore novel non-Hermitian physics [50, 52, 59]. Over the years, ever better techniques of screening experiments as much as possible from any sources of dissipation have been developed, with the goal of observing clean unitary dynamics in isolated quantum systems. This bears the potential to re-introduce channels of engineered dissipation using specifically designed control schemes.

In this section, we present a general method of realizing effective non-Hermitian Hamiltonians, which relies entirely on synthetic sources of dissipation and is designed for accessing the non-Hermitian linear response discussed in Section III for a wide range of observables. The scheme is most conveniently phrased as an application of the quantum Zeno effect [64, 65], and relies on coupling the subsystem of interest to an ancilla system, as depicted in Fig. 3. A measurement of the ancilla population projects the system on the subspace with a definite number of particles in the ancilla. In the quantum Zeno limit, as the measurement frequency tends to infinity, the probability of populating the initially empty ancilla by coupling it to the system vanishes. If, instead, the measurement frequency is finite, there is a finite probability of populating the ancilla. Consequently, the probability of remaining in the empty-ancilla Zeno subspace after the coupling is reduced, as illustrated in Fig. 3. This leakage of probability over time can be described by an effective non-Hermitian Hamiltonian [65, 75, 76] and realizes the desired anti-Hermitian perturbation required for measuring the unequal-time anti-commutator.

Although our scheme can be implemented in various platforms, for the sake of concreteness, we focus here on optical lattices where the ancilla may simply correspond to an auxiliary lattice site. A crucial experimental requirement is the ability to distinguish an empty ancilla from one with non-zero population, which realizes the projection on the empty-ancilla Zeno subspace. This requirement is met, for instance, by modern quantum gas

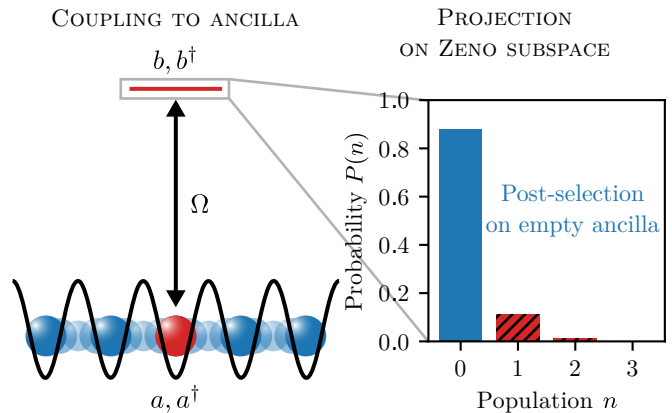


Figure 3. Realization of an effective non-Hermitian Hamiltonian using the quantum Zeno effect. The subsystem of interest, e.g., an optical lattice site, is perturbed by coherently coupling it to an ancilla system, e.g., an auxiliary site in the optical lattice. Thus, the probability of projecting into the empty-ancilla subspace is less than unity, as can be revealed through a post-selected measurement on the condition that no particles are detected in the ancilla. When the projective measurement is performed frequently as compared to the strength of the coherent coupling, the system plus ancilla is in the quantum Zeno regime. Alternatively, the frequent measurements can be substituted by engineered dissipation on the ancilla. In both cases, the leakage out of the empty-ancilla subspace is described by an effective non-Hermitian Hamiltonian, permitting one to design the desired anti-Hermitian perturbation.

microscopes reaching both single-site and single-particle resolution [77, 78].

In what follows, we discuss two variants of our scheme. The first one can be interpreted as a single step in the quantum Zeno evolution and corresponds to a measurement of the non-Hermitian response function in time domain, implementing the delta-like perturbation considered in Section IV. The second one generates a quantum Zeno effect through a continuous coupling to an ancilla that is subject to strong dephasing [66], and represents a measurement of the non-Hermitian dynamic susceptibility in frequency domain.

A. Measurement in time domain

In this subsection, we present a scheme for applying an effective non-Hermitian delta-like perturbation as in Section IV, which allows one to access the unequal-time anti-commutator in Eq. (10) in time domain. The result of such a measurement can then be Fourier transformed according to Eq. (5) or Eq. (15) in order to obtain the susceptibilities entering the FDR (13). To this end, we consider the level scheme depicted in Fig. 3, where the lattice site described by the annihilation and creation operators a and a^\dagger is coherently coupled to an ancilla site with corresponding annihilation and creation

operators b and b^\dagger . This particular level scheme is designed for realizing an effective anti-Hermitian perturbation by the density operator $A = n = a^\dagger a$. By coupling multiple sites to the ancilla, it is possible to construct more general perturbations, but here we focus on the conceptually most straightforward case of density perturbations. For simplicity, we assume that the coupling is resonant and that the ancilla has no internal dynamics. When the coupling is switched on, the total Hamiltonian reads $H = H_0 + H_{\text{cpl}}$, with coupling Hamiltonian $H_{\text{cpl}} = \hbar\Omega(a^\dagger b + b^\dagger a)$ and coupling strength $\Omega > 0$.

The quantum Zeno effect is typically generated through a pulsed series of measurements constraining the system's evolution to the Zeno subspace defined by the projective measurement [65]. However, for the purpose of realizing a singular perturbation at time t_w as in Fig. 1a, it is sufficient to perform only a single step in the Zeno evolution. As in Section IV, we approximate a delta pulse by a rectangular pulse of duration δt , chosen to be much shorter than the characteristic time scales of the Hamiltonian. Let \mathcal{P} denote the projection operator on the empty-ancilla subspace. A single step in the Zeno evolution of the state $\rho(t_w)$ at the waiting time t_w corresponds to a unitary evolution described by the time evolution operator $U(\delta t) = \exp(-iH\delta t/\hbar)$, followed by a projection on the Zeno subspace defined by the projector \mathcal{P} [65]. In this process, the state changes, up to a normalization, as

$$\rho(t_w) \rightarrow \rho'(t_w + \delta t) = \mathcal{P}U(\delta t)\rho(t_w)U^\dagger(\delta t)\mathcal{P}. \quad (17)$$

Subsequently, as illustrated at the top of Fig. 1, the system evolves unitarily under the unperturbed Hamiltonian H_0 up to the final observation time $t > t_w + \delta t$. If the ancilla is unpopulated before the coupling, $\rho(t_w) = \mathcal{P}\rho(t_w)\mathcal{P}$, it can be shown using time-dependent perturbation theory that, to leading order in the effective coupling strength $s = (\Omega\delta t)^2/2$, the unnormalized expectation value of an observable B is given by

$$\text{Tr } B\rho'(t) = \langle B(t) \rangle_0 - s \langle \{B(t), A(t_w)\} \rangle_0 \quad (18)$$

with $A = a^\dagger a$. The details of the derivation are reported in Appendix B. In the linear regime, the probability of detecting no particles in the ancilla after the coupling reads $p(s, t_w) = 1 - 2s \langle A(t_w) \rangle_0$, which can be found by inserting the identity operator for B in Eq. (18). Normalizing Eq. (18) by this probability yields, to leading order in s , the conditional expectation value

$$\langle B(t) \rangle_{\mathcal{P}} = \langle B(t) \rangle_0 - s \left[\langle \{B(t), A(t_w)\} \rangle_0 - 2 \langle B(t) \rangle_0 \langle A(t_w) \rangle_0 \right], \quad (19)$$

representing a post-selected measurement conditioned on the empty ancilla. A comparison with Eqs. (4) and (10) shows that this result effectively corresponds to a linear response after applying the anti-Hermitian perturbation $H_1(t) = -i\hbar s \delta(t - t_w)A$, giving direct access to the symmetrized correlation function (3) via $S_{BA}(t, t_w) =$

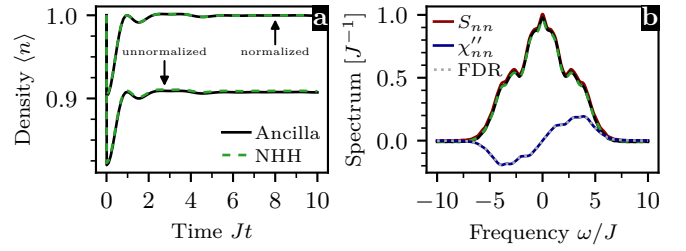


Figure 4. Simulation of the non-Hermitian linear response scheme for measuring density autocorrelations in time domain. The effective non-Hermitian perturbation is generated through a short pulse coupling the system to the ancilla, followed by a projection on the empty-ancilla subspace (see Fig. 3). (a) Unnormalized and normalized responses, corresponding to Eqs. (18) and (19), respectively. The green dashed lines show that the result agrees well with the description in terms of an effective non-Hermitian Hamiltonian (NHH). (b) Correlation spectra extracted from the responses in (a) by Fourier transformation according to Eq. (15), in comparison with the exact FDR (1). Both the effective NHH and the ancilla scheme reproduce the exact correlation spectrum S_{nn} to good accuracy.

$-\langle [B(t)]_{\mathcal{P}} - \langle B(t) \rangle_0] / 2s$. As required in Section III, the perturbation operator $A = a^\dagger a$ is indeed positive semi-definite, in line with the physical intuition that the norm of the state can only decrease through outcoupling followed by a projection.

To benchmark our scheme, we numerically solve the full quantum evolution describing a measurement of the symmetrized density autocorrelation function $S_{nn}(t, t_w)$ ($B = A = n$) for a thermal state $\rho_T = \exp(-H_0/k_B T)/Z(T)$ in a Bose-Hubbard chain of $L = 8$ sites with periodic boundary conditions at unit filling. Here, $Z(T) = \text{Tr} \exp(-H_0/k_B T)$ is the canonical partition sum, and the temperature T is chosen such that the mean energy $\langle H_0 \rangle_T = \text{Tr } H_0 \rho_T$ corresponds to that of a Mott-insulating state. A thermal state is an ideal benchmark for our purposes since the temperature T is known and the FDR is satisfied exactly, so any deviations from the FDR indicate deficiencies of the method.

In Fig. 4a, we show the time trace of the response calculated from a simulation of the ancilla scheme in comparison with a calculation in terms of the corresponding non-Hermitian Hamiltonian. The coupling to the ancilla is applied for a duration $J\delta t = 0.01$ and its strength is chosen such that the effective coupling becomes $s = 0.05$, corresponding to a decay of the norm by about 10%. As can be seen in Fig. 4a, where the unnormalized and normalized responses correspond to Eqs. (18) and (19), respectively, the agreement with the prediction in terms of the non-Hermitian Hamiltonian is remarkable, and leaves room for further enhancing the measurement signal by choosing larger values of s . Since the thermal state is stationary, the waiting time t_w , at which the perturbation is applied, does not matter, and has been chosen as $t_w = 0$. Moreover, the conventions for the dynamic

susceptibilities in Eqs. (5) and (15) are equivalent for a thermal state, such that the correlation spectrum is given by $S_{BA}(\omega) = -\hbar\chi'_{BA}{}^{(\text{NH})}(\omega)$ (see Appendix A). In Fig. 4b, we compare the correlation spectra extracted³ from the responses in Fig. 4a with the exact FDR, directly computed from the unperturbed Hamiltonian (14). Up to small deviations resulting from non-linear effects, our scheme provides an accurate measurement of the correlation spectrum, capable of certifying the validity of the FDR (1).

Experimental considerations and error sources

Many experimental setups such as quantum gas microscopes permit the simultaneous readout of all site populations in a single shot [77, 78]. This is convenient for simultaneously measuring the responses of different observables B , e.g., $B = n_\ell$ for $\ell = 1 \dots L$, to a fixed perturbation A determined by the coupling scheme. In addition, since $[\mathcal{P}, H_0] = 0$, the measurement of the ancilla population can be deferred up to the final observation time t and measured along with the other site populations (cf. Ref. [38]). The projection on the empty-ancilla subspace is then achieved by post-selecting those realizations where no particles were detected in the ancilla. Since the effective coupling s needs to be chosen sufficiently weak to stay within the regime of linear response, the fidelity of the post-selection is typically high (see Fig. 3). However, Eq. (19) shows that there is the usual linear response tradeoff between maximizing the measurement signal (large s) and staying within the perturbative regime where the linear approximation is valid (small s).

One can distinguish two types of detection errors: false positives, i.e., at least one particle is detected in the ancilla, but there is actually none, and false negatives, i.e., no particles are detected, but there is at least one. Let α be the false positive rate and let β be the false negative rate. If the measurement is post-selected on the condition that no particles are detected in the ancilla, which may in some cases be erroneous, the conditional state in Eq. (17) is replaced by $\rho' = (1 - \alpha)\mathcal{P}\rho\mathcal{P} + \beta\mathcal{Q}\rho\mathcal{Q}$, where ρ is the state right after the coupling and before the projection, and $\mathcal{Q} = \mathbb{1} - \mathcal{P}$ is the projector on the subspace with a non-vanishing ancilla population (for simplicity, we do not distinguish different false-negative probabilities within the \mathcal{Q} -subspace since the error due to single occupancies dominates in the linear regime). This shows that false positives lower the measurement fidelity, while false negatives contribute a systematic error to the result, arising from the inadvertent projection on a complemen-

tary subspace (see Appendix B). It is instructive to compare the result in Eq. (19) with the one obtained if no projection on the empty-ancilla subspace is performed, corresponding to the limiting case $\alpha = 0$ and $\beta = 1$, i.e., the measurement apparatus is unable to detect particles in the ancilla. In this case, a simple average over all ancilla populations is obtained, where, to leading order in the effective coupling strength s , only single occupancies of the ancilla site contribute. The change of the expectation value $\Delta B(t) = \langle B(t) \rangle - \langle B(t) \rangle_0$ then reads (see Appendix B)

$$\Delta B(t) = -s\langle \{B(t), n(t_w)\} - 2a^\dagger(t_w)B(t)a(t_w) \rangle_0. \quad (20)$$

The second term on the right-hand side stems from a process where a single particle ends up in the ancilla after the coupling. Post-selecting on the empty ancilla eliminates this undesired contribution, giving access to the unequal-time anti-commutator.

Formal relations to post-selected quantum trajectories and weak measurements

The structure of the second term on the right-hand side of Eq. (20) resembles to the “recycling term” in Lindblad master equations [71, 74]. In fact, coupling to the ancilla can be viewed as an effective dissipative perturbation, $\rho(t_w) \rightarrow \rho(t_w + \delta t) = \rho(t_w) + \delta t\mathcal{D}[\rho(t_w)]$, where $\mathcal{D}[\rho] = \gamma(2a\rho a^\dagger - \{a^\dagger a, \rho\})$ is the Lindblad dissipator with dissipation rate $\gamma = s/\delta t$. This yields Eq. (20) for the expectation value of an observable B after a unitary evolution up to time t . In the quantum trajectories picture [69–71], the Lindblad dissipator $\mathcal{D}[\rho]$ generates an evolution under the non-Hermitian Hamiltonian $H_1 = -i\hbar\gamma a^\dagger a$, subject to quantum jumps described by the “recycling term” $2\gamma a\rho a^\dagger$. By post-selecting on the absence of quantum jumps, it is possible to isolate the pure non-Hermitian evolution [50, 52, 59]. From this point of view, the projection on the empty-ancilla subspace in Eq. (17) can be interpreted as a post-selection on the absence of quantum jumps, i.e., particles hopping to the ancilla. This allows us to eliminate the undesired contribution in Eq. (20) due to the “recycling term” and obtain instead the result in Eq. (19), reflecting a purely non-Hermitian perturbation that gives access to the unequal-time anti-commutator.

Besides the interpretation as a single step in the quantum Zeno evolution or as post-selected quantum trajectories, the outlined scheme also permits an illustrative description as a specifically designed weak measurement [68]. Namely, our scheme can be understood, in analogy to the protocol reported in Ref. [38], as (i) weakly coupling an ancilla to the system at time t_w , (ii) measuring the particle number in the ancilla, (iii) conditioning the system state on the measurement result zero, and (iv) continuing the time evolution up to time t . The first three steps are just a rephrasing of the outcoupling plus projector (see Eq. (17)) that generate the quantum-Zeno

³ Unlike in Section IV, we do not use a frequency filter here, but truncate the Fourier integral in Eq. (15) at $J\Delta t = 10$, where the correlations have sufficiently decayed.

effect and thus the non-Hermitian Hamiltonian. In this sense, the scheme described in this subsection is nothing but a weak measurement, designed in such a way as to enable the extraction of the unequal-time anti-commutator for a broad range of systems and observables.

B. Measurement in frequency domain

We now adapt the scheme presented in the previous subsection to access FDRs directly in frequency domain. From the structure of the general linear response formula (4) it becomes clear that by applying a non-Hermitian perturbation under a suitable periodic modulation $f(t)$ continuously until the final observation time t_f , it is possible to directly measure susceptibilities of the form

$$\chi_{BA}^{(\text{NH})}(t_f, \omega) = \int_{-t_f}^{t_f} d\Delta t \phi_{BA}^{(\text{NH})}(t_f, t_f - \Delta t) e^{i\omega\Delta t}. \quad (21)$$

To this end, it would be natural to consider, instead of a single Zeno step as in Section V A, a pulsed series of measurements, which is the usual setting for the quantum Zeno effect [64, 65, 76]. For the coupling scheme depicted in Fig. 3, repeated projections on the empty-ancilla subspace generate a Zeno effect, preventing a too rapid build-up of population in the ancilla and leading to a gradual leakage of probability out of that Zeno subspace. Thus, the Zeno effect permits us to apply the effective non-Hermitian perturbation over a longer period of time without leaving the linear response regime.

However, implementing the measurement-induced Zeno effect without destroying the sample poses a prohibitive layer of complexity for many experiments. In addition, the required time-dependent modulation of the coupling $\Omega(t)$ necessitates a high measurement frequency to suppress errors from Trotterization. Due to these drawbacks of the *pulsed* Zeno effect, we exploit the *continuous* Zeno effect in what follows. The latter arises in the presence of a strong coupling to an external system, which plays the role of a measurement apparatus and leads to wildly fluctuating phases between the relevant Zeno subspaces [65]. One way of generating such a continuous Zeno effect is by adding engineered classical noise to the system, which has been proposed, e.g., in Ref. [66] to constrain the dynamics of quantum simulators for lattice gauge theories. Here, we apply this idea to realize an effective non-Hermitian Hamiltonian that allows us to directly measure susceptibilities of the form (21).

We consider again the level scheme depicted in Fig. 3, adding classical dephasing noise to the ancilla system. Such a source of noise can be engineered via a rapidly fluctuating effective detuning, e.g., in form of a Zeeman or AC Stark shift, acting on the ancilla only. We assume that the fluctuations are sufficiently fast compared to all relevant physical time scales, such that their effect can be approximated by a Gaussian white noise process $\xi(t)$ satisfying $\langle\langle \xi(t) \rangle\rangle = 0$ and $\langle\langle \xi(t)\xi(t') \rangle\rangle = \delta(t - t')$, where

$\langle\langle \dots \rangle\rangle$ denotes the ensemble average over all noise realizations. For example, using lasers to generate an AC Stark shift, this technical requirement can be fulfilled using acousto-optical devices [79]. The evolution of the density operator $\rho(t)$ can then be described by the stochastic von Neumann equation [66]

$$d\rho = -\frac{i}{\hbar} [H(t), \rho] dt - i\sqrt{2\kappa} [b^\dagger b, \rho] dW(t) \quad (22)$$

with dephasing rate $\kappa > 0$ and Wiener increments $dW(t) = \xi(t) dt$, subject to the Stratonovich interpretation of stochastic calculus [80, 81] (see also Appendix C). The deterministic part of Eq. (22) is governed by the Hamiltonian $H(t) = H_0 + g(t)H_{\text{cpl}}$, where the coupling Hamiltonian $H_{\text{cpl}} = \hbar\Omega(a^\dagger b + b^\dagger a)$ is the same as in Section V A and $g(t)$ is a time-dependent modulation function.

By virtue of stochastic calculus, it can be shown (see Appendix C) that the noise-averaged density operator $\sigma(t) \equiv \langle\langle \rho(t) \rangle\rangle$ satisfies the Lindblad master equation

$$\frac{d}{dt}\sigma = -\frac{i}{\hbar} [H(t), \sigma] - \kappa (\{L^\dagger L, \sigma\} - 2L\sigma L^\dagger) \quad (23)$$

with the Hermitian Lindblad operator $L = b^\dagger b$. The stochastic differential equation (22) represents a diffusive unraveling [82] of the master equation (23). Such diffusive unravelings typically arise in the theory of continuous measurements, where a quantum system is continuously monitored and the resulting measurement back action gives rise to diffusive quantum trajectories [83, 84]. By contrast, in our case, there are no actual measurements involved and Eq. (22) describes a random unitary evolution with pure dephasing [85, 86]. In fact, there exists an infinite number of stochastic unravelings, both diffusive and jump-like, whose ensemble average is described by Eq. (23) [69, 74, 87]. As an alternative to the approach in Eq. (22) using engineered dephasing, we could also start from Eq. (23) with the Lindblad operator $L = b$, describing a spontaneous decay of particles in the ancilla at a decay rate κ . As shown in Appendix C, such a setting gives rise to the same effective non-Hermitian Hamiltonian as considered below.

The quantum Zeno effect is realized in the strong-noise limit $\kappa \rightarrow \infty$, where the build-up of population in the ancilla is suppressed due to the rapidly fluctuating effective detuning [66]. To access the resulting Zeno dynamics, we project the state on the empty-ancilla Zeno subspace [66]. As shown in Appendix C, to leading order perturbation theory, the projected density operator $\sigma_{\mathcal{P}}(t) = \mathcal{P}\sigma(t)\mathcal{P}$ obeys the evolution equation

$$i\hbar \frac{d}{dt}\sigma_{\mathcal{P}} = H_{\text{eff}}(t)\sigma_{\mathcal{P}} - \sigma_{\mathcal{P}}H_{\text{eff}}^\dagger(t), \quad (24)$$

generated by the effective non-Hermitian Hamiltonian $H_{\text{eff}}(t) = H_0 - if(t)A$ with $A = a^\dagger a$ and $f(t) = g^2(t)\hbar\Omega^2/\kappa$. As required in Section III, the perturbation operator A is positive semi-definite and $f(t)$ is non-negative, describing a leakage of probability out of the

empty-ancilla subspace. As before, the projection can be realized via a post-selection on the measurement outcomes where no particles were detected in the ancilla.

It is our goal to extract the reactive part $\chi^{(\text{NH})}$ of the non-Hermitian dynamic susceptibility (21) from the linear response to the effective non-Hermitian Hamiltonian in Eq. (24). For simplicity, we focus on the common case where $\chi^{(\text{NH})}$ corresponds to the real part of Eq. (21), and we consider Hermitian operators A and B such that the response function (10) is real. Due to the non-negativity constraint on $f(t)$, it is not possible to modulate the effective coupling around zero. Instead, we choose the modulation in Eq. (22) as $g(t) = \sqrt{2} \cos(\omega(t_f - t)/2)$, for a fixed final observation time t_f , such that $f(t) = [1 + \cos \omega(t_f - t)] \hbar \Omega^2 / \kappa$. According to Eq. (9), the response is then given by

$$\begin{aligned} \langle B(t_f) \rangle_{\mathcal{P}} &= \langle B(t_f) \rangle_0 + \frac{\hbar \Omega^2}{\kappa} \int_0^{t_f} dt \phi_{BA}^{(\text{NH})}(t_f, t) \\ &+ \frac{\hbar \Omega^2}{\kappa} \int_0^{t_f} dt \phi_{BA}^{(\text{NH})}(t_f, t) \cos \omega(t_f - t), \end{aligned} \quad (25)$$

where $\langle B(t_f) \rangle_{\mathcal{P}} = \text{Tr}[B \sigma_{\mathcal{P}}(t_f)] / \text{Tr} \sigma_{\mathcal{P}}(t_f)$ is the conditional expectation value obtained from post-selection. The first two terms on the right-hand side of Eq. (25) represent the response to a static non-Hermitian perturbation with $g(t) \equiv 1$ and the last term is proportional to the desired real part of Eq. (21), which can be seen after changing the integration variable to $\Delta t = t_f - t$. Thus, it is possible to extract the quantity $\chi^{(\text{NH})}(t_f, \omega)$ for a given probe frequency ω from two linear response measurements, one with a periodic modulation and one with a constant perturbation, the latter being subtracted from the former.

As in Section V A, we benchmark our protocol for extracting the density autocorrelation spectrum $S_{BA}(\omega) = -\hbar \chi^{(\text{NH})}(\omega)$ ($B = A = n$) of a thermal state in a Bose-Hubbard chain. We do so by numerically solving the stochastic von Neumann equation Eq. (22) — the most fundamental equation in our approach — using stochastic Magnus integration [88–90]. By comparing the results of the stochastic simulation to those obtained based on Eqs. (23) and (24), we demonstrate the validity of the approximations underlying the effective description in terms of a non-Hermitian Hamiltonian. To account for the different sensitivities of the responses at different probe frequencies, we parametrize the perturbation strength in terms of the norm decay q due to the effective non-Hermitian Hamiltonian. That is, for each frequency ω , given a fixed final observation time t_f and dephasing rate κ , we adjust the coupling strength Ω such that according to Eq. (8) the norm of the state has decreased by the amount q at the end of the evolution. For a translational invariant system at unit filling, we have $\langle A(t) \rangle_0 = \langle n(t) \rangle_0 = 1$, and therefore $\Omega = [\kappa q / 2 t_f (1 + \text{sinc}(\omega t_f / \pi))]^{1/2}$, where $\text{sinc}(x) = \sin(\pi x) / \pi x$.

In Fig. 5, we show a typical decay of the norm

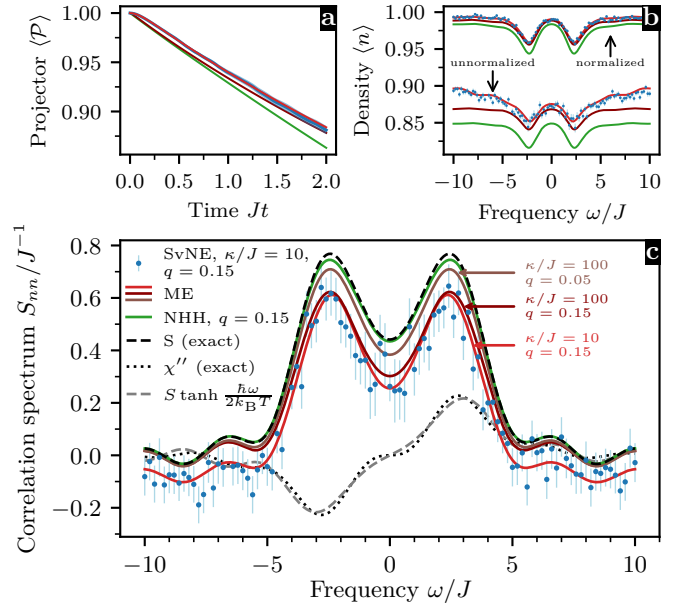


Figure 5. Simulation of the non-Hermitian linear response scheme for measuring the density autocorrelation spectrum in frequency domain. The effective non-Hermitian perturbation is generated through coupling to an ancilla subject to strong engineered dephasing, exploiting the continuous quantum Zeno effect. As indicated by the legend in (c), the simulations are based on the stochastic von Neumann equation (22) (SvNE), the master equation (23) (ME), and the effective non-Hermitian Hamiltonian (24) (NHH). The stochastic simulation has been averaged over 200 realizations, and the error bars show the ensemble standard deviation of the mean. (a) Decrease of the norm resulting from the projection on the empty-ancilla subspace as a function of time for the probe frequency $\omega = 0$ and norm decay $q = 0.15$. A stronger dephasing rate κ improves the agreement between the ME (SvNE) and NHH descriptions at early times, while the deviations at later times are due to non-linear effects. (b) Unnormalized and normalized (conditional) responses, corresponding to Eqs. (7) and (25), respectively, as a function of frequency for a fixed final time $Jt_f = 2$ and norm decay $q = 0.15$. (c) Correlation spectra extracted from the responses in (b) according to Eq. (25), in comparison with the exact FDR (1). The different combinations of the parameters κ and q for the ME simulation show that the agreement with the exact result can be improved by going deeper into the limit of strong dissipation and weak perturbations.

over time due to the effective non-Hermitian perturbation (Fig. 5a), the unnormalized and normalized (conditional) responses corresponding, respectively, to Eqs. (7) and (25) (Fig. 5b), as well as the correlation spectrum in comparison with the exact FDR (Fig. 5c), extracted from simulations based on Eqs. (22) to (24) for a system of $L = 4$ lattice sites. The evolution has been computed up to the final time $Jt_f = 2$, truncating⁴ the Fourier integral in Eq. (25), which for our small system does not

⁴ Continuing the evolution to longer times, the spectrum attains

converge due to revivals. For the stochastic simulation, we have chosen accessible parameters corresponding to a relatively moderate dephasing of strength $\kappa/J = 10$ and a norm decay $q = 0.15$ that results in a good signal-to-noise ratio, but lies slightly beyond the onset of the non-linear regime. As can be seen in Fig. 5, the stochastic simulation based on Eq. (22) agrees with the simulation based on the master equation (23) within the statistical error bars, showing the ensemble standard deviation of the mean for an accessible number of 200 realizations. Moreover, Fig. 5c shows that these parameters already yield the correlation spectrum at a reasonable accuracy suitable for certifying the validity of the FDR (1). The description in terms of the effective non-Hermitian Hamiltonian in Eq. (24) is closer to the exact result than the description in terms of the master equation (23) for the same parameters, revealing that the linear regime is wider for the former than for the latter, which could be remedied through extrapolation. In the effective non-Hermitian description (24), the coupling strength Ω and the dephasing rate κ enter only via the ratio Ω^2/κ , which is proportional to the norm decay q , while these two parameters enter Eqs. (22) and (23) individually. Going deeper into the Zeno limit of large κ improves the validity of Eq. (24) at early times and at larger frequencies, shown in Fig. 5 for $\kappa/J = 100$. Decreasing at the same time the effective coupling strength, as illustrated in Fig. 5 for $q = 0.05$, the agreement between the extracted correlation spectrum and the exact result improves further, which shows that, at the cost of decreasing the signal-to-noise ratio, the exact correlation spectrum can in principle be approximated to arbitrary accuracy.

VI. CONCLUSION

In this work, we have demonstrated how a non-Hermitian perturbation in the linear regime enables access to the unequal-time anti-commutator, which is the missing piece for the direct observation of the FDR in quantum systems. As an illustration, we have discussed how a Bose–Hubbard model after a global quench reaches thermal equilibrium, and we have derived a scenario to generate the required non-Hermitian dynamics in a cold-atom system coupled to an ancillary mode. This proposal provides a concrete scenario for direct observation of the FDR and an unbiased way of probing thermalization dynamics in state-of-the-art experiments on synthetic quantum matter.

The framework is general and can be applied in any non-Hermitian system. It is independent of microscopic details such as interactions, geometry, or particle statistics, and can thus be used with bosons, fermions, or

spins in a wide variety of scenarios. While we have focused on density perturbations in the linear regime, other operators are equally possible by designing suitable non-Hermitian perturbations, and higher orders in the response give access to nested unequal-time anti-commutators of increasing order.

The discussed framework thus provides an array of new possibilities to experimentally — and also numerically [25] — characterize quantum systems in and out of thermal equilibrium.

ACKNOWLEDGMENTS

We thank J. Berges, M. Gärttner, S. Lannig, M. K. Oberthaler, A. Piñeiro Orioli, J. Reichstetter, and A. Salzinger for discussions, and we acknowledge support by Provincia Autonoma di Trento and the ERC Starting Grant StrEnQTh (project ID 804305). This work is part of Q@TN — Quantum Science and Technology in Trento — and the Collaborative Research Centre ISOQUANT (project ID 273811115). The authors acknowledge support by the state of Baden-Württemberg through bwHPC.

Appendix A: Derivation of the non-Hermitian linear response formula

To derive Eq. (7), we first transform to the interaction picture with respect to the unperturbed (Hermitian) Hamiltonian H_0 . The von Neumann equation (6) then reads

$$\frac{d}{dt}\tilde{\rho} = -\frac{i}{\hbar}\{\tilde{H}_1(t), \tilde{\rho}\}, \quad (\text{A1})$$

where $\tilde{\rho}(t) = e^{iH_0t/\hbar}\rho(t)e^{-iH_0t/\hbar}$ is the density operator and $\tilde{H}_1(t) = -if(t)\tilde{A}(t)$ with $\tilde{A}(t) = e^{iH_0t/\hbar}Ae^{-iH_0t/\hbar}$ is the anti-Hermitian perturbation in the interaction picture. This equation can equivalently be expressed in integral form as

$$\tilde{\rho}(t) = \tilde{\rho}(0) - \frac{i}{\hbar}\int_0^t dt' \{\tilde{H}_1(t'), \tilde{\rho}(t')\} \quad (\text{A2})$$

with $\tilde{\rho}(0) = \rho_0$. To linear order in the perturbation, we can replace $\tilde{\rho}(t')$ in the integrand by ρ_0 , yielding

$$\tilde{\rho}(t) = \rho_0 - \frac{1}{\hbar}\int_0^t dt' \{\tilde{A}_1(t'), \rho_0\}f(t'). \quad (\text{A3})$$

The expectation value of an observable B can be computed in the interaction picture as $\langle B(t) \rangle = \text{Tr} \tilde{B}(t)\tilde{\rho}(t)$, where $\tilde{B}(t) = e^{iH_0t/\hbar}Be^{-iH_0t/\hbar}$. Inserting Eq. (A3) into this expression and using the cyclic property of the trace leads to the result in Eq. (7).

To show that $S_{BA}(\tau, \omega) = -\hbar\chi'_{BA}(\text{NH})(\tau, \omega)$, we first note that the symmetric correlation function (3) obeys

more structure, but the validity of the FDR is only marginally affected by the chosen truncation.

the symmetry relation $S_{BA}(t, t') = S_{AB}(t', t)$. In what follows, we use the short-hand notation $S_{BA}(\tau, \Delta t) = S_{BA}(t = \tau + \Delta t/2, t' = \tau - \Delta t/2)$. Then, the aforementioned identity reads $S_{BA}(\tau, \Delta t) = S_{AB}(\tau, -\Delta t)$. This allows us to express the correlation spectrum as

$$\begin{aligned} S_{BA}(\tau, \omega) &= \int_{-2\tau}^{2\tau} d\Delta t S_{BA}(\tau, \Delta t) e^{i\omega\Delta t} \\ &= \int_0^{2\tau} d\Delta t S_{BA}(\tau, \Delta t) e^{i\omega\Delta t} \\ &\quad + \int_0^{2\tau} d\Delta t S_{AB}(\tau, \Delta t) e^{-i\omega\Delta t}. \end{aligned} \quad (\text{A4})$$

Using further Eq. (10), noting that the Heaviside step function allows us to extend the integration domain to negative Δt , as well as the definition of the generalized susceptibility (5), we arrive at

$$\begin{aligned} S_{BA}(\tau, \omega) &= -\frac{\hbar}{2} \int_{-2\tau}^{2\tau} d\Delta t \phi_{BA}^{(\text{NH})}(\tau, \Delta t) e^{i\omega\Delta t} \\ &\quad - \frac{\hbar}{2} \int_{-2\tau}^{2\tau} d\Delta t \phi_{AB}^{(\text{NH})}(\tau, \Delta t) e^{-i\omega\Delta t} \\ &= -\frac{\hbar}{2} \left[\chi_{BA}^{(\text{NH})}(\tau, \omega) + \chi_{AB}^{(\text{NH})}(\tau, -\omega) \right] \\ &= -\hbar \chi'_{BA}^{(\text{NH})}(\tau, \omega). \end{aligned} \quad (\text{A5})$$

By contrast, if we consider the Fourier transform at fixed waiting time t_w as in Eq. (15), the integrand $S_{BA}(t_w + \Delta t, t_w)$ does not possess a symmetry with respect to the relative time Δt in general. Thus, out of equilibrium, we generally have $S_{BA}(t_w, \omega) \neq -\hbar \chi'_{BA}^{(\text{NH})}(t_w, \omega)$, but this relation is restored once the system reaches a stationary state.

Appendix B: Derivation of the protocol for measuring unequal-time anti-commutators

In this appendix, we use time-dependent perturbation theory to derive Eqs. (19) and (20), describing, respectively, the conditional and unconditional response after coupling the system to the ancilla as depicted in Fig. 3.

The linear response protocol starts by evolving the initial state ρ_0 under the Hamiltonian H_0 up to the waiting time t_w , at which the perturbation is applied. Before the coupling, the state is given by $\rho(t_w) = e^{-iH_0 t_w/\hbar} \rho_0 e^{iH_0 t_w/\hbar}$. In Section V A, we have approximated a delta-like perturbation as a rectangular pulse of duration δt . Here, we consider a slightly more general scenario, where we allow for an arbitrarily shaped pulse $g(t)$ with compact support on the interval $[t_w, t_w + \delta t]$, normalized such that $\int_{t_w}^{t_w + \delta t} dt g(t) = \delta t$. The corresponding Hamiltonian reads $H(t) = H_0 + g(t)H_{\text{cpl}}$ with $H_{\text{cpl}} = \hbar\Omega(a^\dagger b + b^\dagger a)$. It is convenient to work in the interaction picture with respect to the unperturbed Hamiltonian H_0 . Time evolution is then governed by the von Neumann equation

$$i\hbar \frac{d}{dt} \tilde{\rho} = [g(t)\tilde{H}_{\text{cpl}}(t), \tilde{\rho}], \quad (\text{B1})$$

where $\tilde{\rho}(t) = e^{iH_0 t/\hbar} \rho(t) e^{-iH_0 t/\hbar}$ and $\tilde{H}_{\text{cpl}}(t) = \hbar\Omega [\tilde{a}^\dagger(t)b + b^\dagger \tilde{a}(t)]$ with $\tilde{a}(t) = e^{iH_0 t/\hbar} a e^{-iH_0 t/\hbar}$ denote, respectively, the density operator and the coupling Hamiltonian in the interaction picture. Rewriting Eq. (B1) as an integral equation and substituting the left-hand side into the right-hand side, we arrive at

$$\tilde{\rho}(t_w + \delta t) = \tilde{\rho}(t_w) - \frac{i}{\hbar} \int_{t_w}^{t_w + \delta t} dt g(t) [\tilde{H}_{\text{cpl}}(t), \tilde{\rho}(t_w)] - \frac{1}{\hbar^2} \int_{t_w}^{t_w + \delta t} dt g(t) \int_{t_w}^t dt' g(t') [\tilde{H}_{\text{cpl}}(t), [\tilde{H}_{\text{cpl}}(t'), \tilde{\rho}(t')]]. \quad (\text{B2})$$

If the pulse duration δt is much shorter than the characteristic time scales of H_0 , we can approximate $\tilde{\rho}(t) \approx \tilde{\rho}(t_w)$ and $\tilde{H}_{\text{cpl}}(t) \approx \tilde{H}_{\text{cpl}}(t') \approx \tilde{H}_{\text{cpl}}(t_w)$ in the integrands, yielding, up to second order in δt , the result

$$\begin{aligned} \tilde{\rho}(t_w + \delta t) &\approx \tilde{\rho}(t_w) - \frac{i}{\hbar} \delta t [\tilde{H}_{\text{cpl}}(t_w), \tilde{\rho}(t_w)] \\ &\quad - \frac{\delta t^2}{2\hbar^2} (\{ \tilde{H}_{\text{cpl}}^2(t_w), \tilde{\rho}(t_w) \} \\ &\quad - 2\tilde{H}_{\text{cpl}}(t_w) \tilde{\rho}(t_w) \tilde{H}_{\text{cpl}}(t_w)). \end{aligned} \quad (\text{B3})$$

We require the ancilla to be empty before the coupling. More specifically, we assume that the combined state of system and ancilla at the waiting time t_w is given by the product state $\tilde{\rho}(t_w) = \tilde{\rho}_S(t_w) \otimes \tilde{\rho}_A$, where the ancilla is in

the pure vacuum state $\tilde{\rho}_A = |0\rangle\langle 0|$. Inserting this state into Eq. (B3), we obtain

$$\begin{aligned} \tilde{\rho}(t_w + \delta t) &= \tilde{\rho}_S(t_w) \otimes |0\rangle\langle 0| \\ &\quad - i\Omega\delta t [\tilde{a}(t_w)\tilde{\rho}_S(t_w) \otimes |1\rangle\langle 0| - \text{h.c.}] \\ &\quad - \frac{(\Omega\delta t)^2}{2} \left[\{ \tilde{n}(t_w), \tilde{\rho}_S(t_w) \} \otimes |0\rangle\langle 0| \right. \\ &\quad \quad - 2\tilde{a}(t_w)\tilde{\rho}_S(t_w)\tilde{a}^\dagger(t_w) \otimes |1\rangle\langle 1| \\ &\quad \quad \left. + \sqrt{2} (\tilde{a}^2(t_w)\tilde{\rho}_S(t_w) \otimes |2\rangle\langle 0| + \text{h.c.}) \right], \end{aligned} \quad (\text{B4})$$

where $\tilde{n}(t_w) = \tilde{a}^\dagger(t_w)\tilde{a}(t_w)$ is the number operator and h.c. denotes the Hermitian conjugate.

After coupling the system to the ancilla, a single step in the Zeno evolution is completed by measuring the pop-

ulation of the ancilla, projecting the state on a subspace with a definite number of particles in the ancilla. Let $\mathcal{P}_n = \mathbf{1} \otimes |n\rangle\langle n|$ be the projection operator on the subspace with n particles in the ancilla. Since $[\mathcal{P}_n, H_0] = 0$, the measurement can optionally be deferred up to the final observation time. The projected states read

$$\mathcal{P}_0 \tilde{\rho}(t_w + \delta t) \mathcal{P}_0 = (\tilde{\rho}_S(t_w) - s \{ \tilde{n}(t_w), \tilde{\rho}_S(t_w) \}) \otimes |0\rangle\langle 0|, \quad (\text{B5a})$$

$$\mathcal{P}_1 \tilde{\rho}(t_w + \delta t) \mathcal{P}_1 = 2s \tilde{a}(t_w) \tilde{\rho}_S(t_w) \tilde{a}^\dagger(t_w) \otimes |1\rangle\langle 1|, \quad (\text{B5b})$$

where $s = (\Omega \delta t)^2 / 2$ is the effective coupling strength, and $\mathcal{P}_n \tilde{\rho}(t_w + \delta t) \mathcal{P}_n = 0$ for $n \geq 2$, up to second order in δt . The probability of detecting n particles in the ancilla is then given by $p(n) = \text{Tr} \mathcal{P}_n \tilde{\rho}(t_w + \delta t) \mathcal{P}_n$, which yields

$$p(0) = 1 - 2s \langle n(t_w) \rangle_0, \quad (\text{B6a})$$

$$p(1) = 2s \langle n(t_w) \rangle_0, \quad (\text{B6b})$$

and $p(n \geq 2) = 0$, up to second order in δt . Here, we have used $\text{Tr} \tilde{\rho}(t_w) \tilde{n}(t_w) = \text{Tr} \rho_0 n(t_w) = \langle n(t_w) \rangle_0$.

According to Lüders' rule [91], the conditional state, given that n particles have been detected in the ancilla, is obtained by normalizing the projected states (B5) by the respective probabilities (B6), i.e., $\tilde{\rho}(t_w + \delta t|n) = \mathcal{P}_n \tilde{\rho}(t_w + \delta t) \mathcal{P}_n / p(n)$. Up to leading order in s , we find

$$\tilde{\rho}(t_w + \delta t|0) = \tilde{\rho}(t_w) - s \left[\{ \tilde{n}(t_w), \tilde{\rho}(t_w) \} - 2 \langle n(t_w) \rangle_0 \tilde{\rho}(t_w) \right], \quad (\text{B7a})$$

$$\tilde{\rho}(t_w + \delta t|1) = \frac{\tilde{a}(t_w) \tilde{\rho}(t_w) \tilde{a}^\dagger(t_w)}{\langle n(t_w) \rangle_0}, \quad (\text{B7b})$$

where we have discarded (or traced out) the ancilla and omitted the subscripts indicating system density operators. By contrast, if the ancilla population is not measured or if the measurement outcomes are ignored, the state after the coupling is instead described by the unconditional density operator

$$\begin{aligned} \tilde{\rho}(t_w + \delta t) &= \sum_n p(n) \tilde{\rho}(t_w + \delta t|n) \\ &= \tilde{\rho}(t_w) - s \left(\{ \tilde{n}(t_w), \tilde{\rho}(t_w) \} - 2 \tilde{a}(t_w) \tilde{\rho}(t_w) \tilde{a}^\dagger(t_w) \right), \end{aligned} \quad (\text{B8})$$

which can be obtained directly from Eq. (B4) after tracing out the ancilla.

For times $t > t_w + \delta t$, the coupling is switched off and the system evolves solely under the Hamiltonian H_0 . According to Eq. (B1), this evolution is trivial in the interaction picture, such that $\tilde{\rho}(t) = \tilde{\rho}(t_w + \delta t)$. The (unnormalized) expectation value of an observable B with respect to the state (B5a) projected on the empty-ancilla subspace reads

$$\begin{aligned} \text{Tr} \tilde{B}(t) \mathcal{P}_0 \tilde{\rho}(t) \mathcal{P}_0 &= \text{Tr} \tilde{B}(t) \tilde{\rho}(t_w) \\ &\quad - s \text{Tr} \tilde{B}(t) \{ \tilde{n}(t_w), \tilde{\rho}(t_w) \} \\ &= \text{Tr} B(t) \rho_0 \\ &\quad - s \text{Tr} B(t) \{ n(t_w), \rho_0 \} \\ &= \langle B(t) \rangle_0 - s \langle \{ B(t), n(t_w) \} \rangle_0, \end{aligned} \quad (\text{B9})$$

where, in the second step, we have transformed from the interaction picture to the Heisenberg picture, and in the last step, we have used the cyclic property of the trace. This is the result reported in Eq. (18) in the main text. For the conditional state (B7a), we recover Eq. (18), which describes a post-selected measurement conditioned on the empty ancilla.

If we were to post-select on the condition that a single particle is detected in the ancilla, corresponding to the conditional state Eq. (B7b), we would instead obtain

$$\text{Tr} \tilde{B}(t) \tilde{\rho}(t|1) = \frac{\langle a^\dagger(t_w) B(t) a(t_w) \rangle_0}{\langle n(t_w) \rangle_0}. \quad (\text{B10})$$

This quantity contributes a systematic error in the case of faulty detection with false negatives (see the discussion in Section V A). From the derivation in this appendix it becomes clear that, up to second order in δt , i.e., up to linear order in the effective coupling strength s , the error is dominated by single occupancies of the ancilla site. Finally, the unconditional expectation value (20) follows from Eq. (B8). This shows that post-selection is essential in order to remove the undesired contribution in form of the ‘‘recycling term’’ due to Eq. (B7b), enabling access to the unequal-time anti-commutator.

Appendix C: From engineered dissipation to an effective non-Hermitian Hamiltonian

The Gaussian white noise process $\xi(t)$ considered in Section V B can be viewed as the idealization of a smooth physical noise process with finite correlation time, arising, for example, from a rapidly fluctuating electric or magnetic field. As such, it is appropriate to interpret the stochastic von Neumann equation Eq. (22) as a stochastic differential equation (SDE) in Stratonovich form, which obeys the rules of ordinary calculus [80, 81]. In addition, in the form of Eq. (22), unitary evolution of each realization ($d \text{Tr} \rho(t) / dt = 0$) is only guaranteed if the Stratonovich interpretation is used [85].

The master equation Eq. (23) can be derived from the stochastic von Neumann equation Eq. (22) by averaging over all noise realizations. However, in the Stratonovich interpretation, the Wiener increments $dW(t)$ and the stochastic variable $\rho(t)$ are not statistically independent at equal times, i.e., $\langle \langle \rho(t) dW(t) \rangle \rangle \neq 0$ in general. To arrive at Eq. (23), it is therefore advantageous to convert Eq. (22) to an Itô SDE [80, 81]. According to the conversion rules, the linear Stratonovich SDE $d\rho = L_0(t) \rho dt + L_1(t) \rho dW$ is equivalent to the linear Itô SDE $d\rho = [L_0(t) + L_1^2(t)/2] \rho dt + L_1(t) \rho dW$. In the case of Eq. (22), L_0 and L_1 are given by the Liouvillian superoperators $L_0(t) \rho = -i[H(t), \rho] / \hbar$ and $L_1 \rho = -i\sqrt{2\kappa} [b^\dagger b, \rho]$, respectively. Thus Eq. (22) is

equivalent to the Itô SDE

$$d\rho = -\frac{i}{\hbar}[H(t), \rho] dt - \kappa(\{L^\dagger L, \rho\} - 2L\rho L^\dagger) dt - i\sqrt{2\kappa}[b^\dagger b, \rho] dW \quad (\text{C1})$$

with $L = b^\dagger b$. Since the solution of an Itô SDE is non-anticipating [80, 81], we have $\langle\langle \rho(t) dW(t) \rangle\rangle = 0$. Therefore, taking the ensemble average of Eq. (C1), the stochastic term vanishes, and the noise-averaged density operator $\sigma(t) = \langle\langle \rho(t) \rangle\rangle$ obeys the master equation (23).

To derive the effective non-Hermitian Hamiltonian governing the evolution in Eq. (24), following Ref. [66], we consider the strong noise limit of Eq. (23) projected on the empty-ancilla subspace. It is convenient to work in the interaction picture, i.e, in a rotating frame with respect to the unperturbed Hamiltonian H_0 . Equation (23) then reads

$$\frac{d}{dt}\tilde{\sigma} = -\frac{i}{\hbar}[\tilde{H}_{\text{cpl}}(t), \tilde{\sigma}] - \kappa(\{L^\dagger L, \tilde{\sigma}\} - 2L\tilde{\sigma}L^\dagger), \quad (\text{C2})$$

where $\tilde{\sigma}(t) = e^{iH_0 t/\hbar}\sigma(t)e^{-iH_0 t/\hbar}$ and $\tilde{H}_{\text{cpl}}(t) = g(t)\hbar\Omega[\tilde{a}^\dagger(t)b + b^\dagger\tilde{a}(t)]$ with $\tilde{a}(t) = e^{iH_0 t/\hbar}ae^{-iH_0 t/\hbar}$. The operators b and b^\dagger as well as the Lindblad operators remain unchanged as they act on the ancilla only and therefore commute with H_0 .

We now use the projection operator on the empty-ancilla subspace $\mathcal{P} = \mathcal{P}_0$ as well as its complement $\mathcal{Q} = \mathbb{1} - \mathcal{P}$ to derive coupled equations for the populations $\tilde{\sigma}_{\mathcal{P}\mathcal{P}} = \mathcal{P}\tilde{\sigma}\mathcal{P}$ and $\tilde{\sigma}_{\mathcal{Q}\mathcal{Q}} = \mathcal{Q}\tilde{\sigma}\mathcal{Q}$ of the two subspaces, as well as for their coherences $\tilde{\sigma}_{\mathcal{P}\mathcal{Q}} = \mathcal{P}\tilde{\sigma}\mathcal{Q}$ and $\tilde{\sigma}_{\mathcal{Q}\mathcal{P}} = \mathcal{Q}\tilde{\sigma}\mathcal{P}$. The projection operators are Hermitian and satisfy the properties $\mathcal{P}^2 = \mathcal{P}$, $\mathcal{Q}^2 = \mathcal{Q}$, $\mathcal{P}\mathcal{Q} = \mathcal{Q}\mathcal{P} = 0$, as well as $[\mathcal{P}, H_0] = [\mathcal{Q}, H_0] = 0$, the latter following from the fact that H_0 does not change the number of particles in the ancilla. Furthermore, since \mathcal{P} projects on the empty-ancilla subspace, we have $b\mathcal{P} = \mathcal{P}b^\dagger = 0$. Applying the projectors \mathcal{P} and \mathcal{Q} to Eq. (C2) from the left and from the right yields the coupled system of equations

$$\frac{d}{dt}\tilde{\sigma}_{\mathcal{P}\mathcal{P}} = -\frac{i}{\hbar}(\tilde{H}_{\mathcal{P}\mathcal{Q}}\tilde{\sigma}_{\mathcal{Q}\mathcal{P}} - \tilde{\sigma}_{\mathcal{P}\mathcal{Q}}\tilde{H}_{\mathcal{Q}\mathcal{P}}), \quad (\text{C3a})$$

$$\begin{aligned} \frac{d}{dt}\tilde{\sigma}_{\mathcal{P}\mathcal{Q}} &= -\frac{i}{\hbar}(\tilde{H}_{\mathcal{P}\mathcal{Q}}\tilde{\sigma}_{\mathcal{Q}\mathcal{Q}} - \tilde{\sigma}_{\mathcal{P}\mathcal{P}}\tilde{H}_{\mathcal{P}\mathcal{Q}}) \\ &+ \frac{i}{\hbar}\tilde{\sigma}_{\mathcal{P}\mathcal{Q}}\mathcal{Q}\tilde{H}_{\text{cpl}}\mathcal{Q} - \kappa\tilde{\sigma}_{\mathcal{P}\mathcal{Q}}\mathcal{Q}L^\dagger L\mathcal{Q}, \end{aligned} \quad (\text{C3b})$$

$$\begin{aligned} \frac{d}{dt}\tilde{\sigma}_{\mathcal{Q}\mathcal{P}} &= -\frac{i}{\hbar}(\tilde{H}_{\mathcal{Q}\mathcal{P}}\tilde{\sigma}_{\mathcal{P}\mathcal{P}} - \tilde{\sigma}_{\mathcal{Q}\mathcal{Q}}\tilde{H}_{\mathcal{Q}\mathcal{P}}) \\ &- \frac{i}{\hbar}\mathcal{Q}\tilde{H}_{\text{cpl}}\mathcal{Q}\tilde{\sigma}_{\mathcal{Q}\mathcal{P}} - \kappa\mathcal{Q}L^\dagger L\mathcal{Q}\tilde{\sigma}_{\mathcal{Q}\mathcal{P}}, \end{aligned} \quad (\text{C3c})$$

$$\begin{aligned} \frac{d}{dt}\tilde{\sigma}_{\mathcal{Q}\mathcal{Q}} &= -\frac{i}{\hbar}(\tilde{H}_{\mathcal{Q}\mathcal{P}}\tilde{\sigma}_{\mathcal{P}\mathcal{Q}} - \tilde{\sigma}_{\mathcal{Q}\mathcal{P}}\tilde{H}_{\mathcal{P}\mathcal{Q}}) \\ &- \frac{i}{\hbar}[\mathcal{Q}\tilde{H}_{\text{cpl}}\mathcal{Q}, \tilde{\sigma}_{\mathcal{Q}\mathcal{Q}}] \\ &- \kappa\mathcal{Q}(\{L^\dagger L, \tilde{\sigma}_{\mathcal{Q}\mathcal{Q}}\} - 2L\tilde{\sigma}_{\mathcal{Q}\mathcal{Q}}L^\dagger)\mathcal{Q}, \end{aligned} \quad (\text{C3d})$$

where the operators $\tilde{H}_{\mathcal{P}\mathcal{Q}}(t) = g(t)\hbar\Omega\mathcal{P}\tilde{a}^\dagger(t)b\mathcal{Q}$ and $\tilde{H}_{\mathcal{Q}\mathcal{P}}(t) = g(t)\hbar\Omega\mathcal{Q}b^\dagger\tilde{a}(t)\mathcal{P}$ mix the two subspaces. In deriving Eq. (C2), we have considered the engineered dephasing scenario described by the stochastic von Neumann equation (22), in which case the Lindblad operator $L = b^\dagger b$ is Hermitian and the projectors commute with L . In the alternative setting, where the ancilla is subject to spontaneous decay, the Lindblad operator is given by $L = b$ and does not commute with the projectors. In this case, Eqs. (C3a) to (C3c) receive an additional contribution from the ‘‘recycling terms’’ $2\kappa b\tilde{\sigma}_{\mathcal{Q}\mathcal{Q}}b^\dagger$, whose effect is to incoherently remove particles from the ancilla. Since these terms are proportional to $\tilde{\sigma}_{\mathcal{Q}\mathcal{Q}}$, which is initially zero and whose growth is suppressed by the Zeno effect, their presence does not change the following line of arguments. Nonetheless, it is possible to get rid of these terms completely by keeping track of all the modes the ancilla decays to and post-selecting on the condition that the ancilla plus these additional modes are empty. To see this, we can assume that the ancilla decays only to a single mode with associated annihilation and creation operators c and c^\dagger . The corresponding Lindblad operator $L = c^\dagger b$ now conserves the number of particles in the ancilla plus the extra mode. Consequently, the contribution from the ‘‘recycling terms’’ to Eqs. (C3a) to (C3c) vanishes due to the action of the projector \mathcal{P} .

We now consider the strong noise limit of Eq. (C3). The terms on the right-hand side of the equations for the coherences (C3b) and (C3c) rotate at characteristic frequencies of the unperturbed Hamiltonian H_0 via $\tilde{a}(t) = e^{iH_0 t/\hbar}ae^{-iH_0 t/\hbar}$ as well as via the modulation function $g(t)$, whose role is to probe dynamic correlations in the system at a given frequency. In contrast, the terms proportional to the dissipation rate κ cause a damping of the coherences. If κ is sufficiently large, in particular, if it is much larger than the characteristic frequencies of H_0 , we can make the approximation that the coherences are instantaneously damped to a momentary equilibrium state given by $d\tilde{\sigma}_{\mathcal{P}\mathcal{Q}}/dt \approx 0$ (and analogously for $\tilde{\sigma}_{\mathcal{Q}\mathcal{P}}$). This allows us to adiabatically eliminate the fast incoherent dynamics and to solve Eqs. (C3b) and (C3c) for the coherences. To leading order in Ω/κ , we find

$$\tilde{\sigma}_{\mathcal{P}\mathcal{Q}} = -\frac{i}{\hbar\kappa}(\tilde{H}_{\mathcal{P}\mathcal{Q}}\tilde{\sigma}_{\mathcal{Q}\mathcal{Q}} - \tilde{\sigma}_{\mathcal{P}\mathcal{P}}\tilde{H}_{\mathcal{P}\mathcal{Q}})(\mathcal{Q}L^\dagger L\mathcal{Q})^{-1}, \quad (\text{C4a})$$

$$\tilde{\sigma}_{\mathcal{Q}\mathcal{P}} = -\frac{i}{\hbar\kappa}(\mathcal{Q}L^\dagger L\mathcal{Q})^{-1}(\tilde{H}_{\mathcal{Q}\mathcal{P}}\tilde{\sigma}_{\mathcal{P}\mathcal{P}} - \tilde{\sigma}_{\mathcal{Q}\mathcal{Q}}\tilde{H}_{\mathcal{Q}\mathcal{P}}), \quad (\text{C4b})$$

where $(\dots)^{-1}$ denotes the Moore–Penrose pseudoinverse. To leading order in Ω/κ , we can furthermore neglect the terms proportional to $\tilde{\sigma}_{\mathcal{Q}\mathcal{Q}}$, which is initially zero and grows, according to Eqs. (C3d) and (C4), only slowly at a rate Ω^2/κ . This suppression of the growth of population in the ancilla is precisely a manifestation of the Zeno effect. Thus, plugging Eq. (C4) into Eq. (C3a), we obtain

$$\frac{d}{dt}\tilde{\sigma}_{\mathcal{P}\mathcal{P}} = -\frac{i}{\hbar}\{\tilde{H}_{\text{eff}}(t), \tilde{\sigma}_{\mathcal{P}\mathcal{P}}\} \quad (\text{C5})$$

with the effective non-Hermitian Hamiltonian

$$\tilde{H}_{\text{eff}}(t) = -ig^2(t) \frac{\hbar\Omega^2}{\kappa} \mathcal{P} \tilde{a}^\dagger(t) b (QL^\dagger LQ)^{-1} b^\dagger \tilde{a}(t) \mathcal{P}. \quad (\text{C6})$$

Due to the action of the projector \mathcal{P} in this expression, the pseudoinverse acts only on states with ex-

actly one particle in the ancilla, where it reduces to a multiplication by unity. Thus, the effective non-Hermitian Hamiltonian takes the simple form $\tilde{H}_{\text{eff}}(t) = -ig^2(t) \hbar\Omega^2 \mathcal{P} \tilde{a}^\dagger(t) \tilde{a}(t) \mathcal{P} / \kappa$. Finally, Eq. (24) follows after transforming back to the non-rotating frame.

-
- [1] R. J. Glauber, The quantum theory of optical coherence, *Phys. Rev.* **130**, 2529 (1963).
- [2] M. O. Scully and M. S. Zubairy, *Quantum Optics* (Cambridge University Press, 1997).
- [3] J. Jensen and A. R. Mackintosh, *Rare Earth Magnetism: Structures and Excitations*, International Series of Monographs on Physics (Clarendon Press, Oxford, 1991).
- [4] P. Coleman, *Introduction to Many-Body Physics* (Cambridge University Press, Cambridge, 2015).
- [5] J. Berges, K. Boguslavski, S. Schlichting, and R. Venugopalan, Universality far from equilibrium: From superfluid Bose gases to heavy-ion collisions, *Phys. Rev. Lett.* **114**, 061601 (2015), arXiv:1408.1670 [hep-ph].
- [6] A. Piñeiro Orioli, K. Boguslavski, and J. Berges, Universal self-similar dynamics of relativistic and nonrelativistic field theories near nonthermal fixed points, *Phys. Rev. D* **92**, 025041 (2015), arXiv:1503.02498 [hep-ph].
- [7] C.-M. Schmied, A. N. Mikheev, and T. Gasenzer, Nonthermal fixed points: Universal dynamics far from equilibrium, *International Journal of Modern Physics A* **34**, 1941006 (2019), arXiv:1810.08143 [cond-mat.quant-gas].
- [8] A. Chatrchyan, K. T. Geier, M. K. Oberthaler, J. Berges, and P. Hauke, Analog reheating of the early universe in the laboratory, arXiv:2008.02290 [cond-mat.quant-gas] (2020).
- [9] B. Sciolla, D. Poletti, and C. Kollath, Two-time correlations probing the dynamics of dissipative many-body quantum systems: Aging and fast relaxation, *Phys. Rev. Lett.* **114**, 170401 (2015), arXiv:1407.4939 [cond-mat.quant-gas].
- [10] J. C. Halimeh and M. F. Maghrebi, Quantum aging and dynamical universality in the long-range $o(n \rightarrow \infty)$ model, arXiv:2008.08583 [cond-mat.stat-mech] (2020).
- [11] F. Arceri, F. P. Landes, L. Berthier, and G. Biroli, Glasses and aging: A statistical mechanics perspective, arXiv:2006.09725 [cond-mat.stat-mech] (2020).
- [12] T. V. Zache, N. Mueller, J. T. Schneider, F. Jendrzejewski, J. Berges, and P. Hauke, Dynamical topological transitions in the massive Schwinger model with a θ term, *Phys. Rev. Lett.* **122**, 050403 (2019), arXiv:1808.07885 [quant-ph].
- [13] J. M. Deutsch, Quantum statistical mechanics in a closed system, *Phys. Rev. A* **43**, 2046 (1991).
- [14] M. Srednicki, Chaos and quantum thermalization, *Phys. Rev. E* **50**, 888 (1994), arXiv:cond-mat/9403051 [cond-mat].
- [15] C. Gogolin and J. Eisert, Equilibration, thermalisation, and the emergence of statistical mechanics in closed quantum systems, *Reports on Progress in Physics* **79**, 056001 (2016), arXiv:1503.07538 [quant-ph].
- [16] L. D'Alessio, Y. Kafri, A. Polkovnikov, and M. Rigol, From quantum chaos and eigenstate thermalization to statistical mechanics and thermodynamics, *Adv. Phys.* **65**, 239 (2016), arXiv:1509.06411 [cond-mat.stat-mech].
- [17] J. M. Deutsch, Eigenstate thermalization hypothesis, *Rep. Progr. Phys.* **81**, 082001 (2018), arXiv:1805.01616 [quant-ph].
- [18] H. B. Callen and T. A. Welton, Irreversibility and generalized noise, *Phys. Rev.* **83**, 34 (1951).
- [19] R. Kubo, Statistical-mechanical theory of irreversible processes. I. General theory and simple applications to magnetic and conduction problems, *J. Phys. Soc. Jpn.* **12**, 570 (1957).
- [20] R. Kubo, The fluctuation-dissipation theorem, *Rep. Prog. Phys.* **29**, 255 (1966).
- [21] A. Einstein, Über die von der molekularkinetischen Theorie der Wärme geforderte Bewegung von in ruhenden Flüssigkeiten suspendierten Teilchen, *Ann. Phys.* **17**, 549 (1905).
- [22] L. Foini, L. F. Cugliandolo, and A. Gambassi, Fluctuation-dissipation relations and critical quenches in the transverse field Ising chain, *Phys. Rev. B* **84**, 212404 (2011), arXiv:1107.5956 [cond-mat.stat-mech].
- [23] L. Foini, L. F. Cugliandolo, and A. Gambassi, Dynamic correlations, fluctuation-dissipation relations, and effective temperatures after a quantum quench of the transverse field Ising chain, *J. Stat. Mech. Theory Exp.* **2012**, P09011 (2012), arXiv:1207.1650 [cond-mat.stat-mech].
- [24] E. Khatami, G. Pupillo, M. Srednicki, and M. Rigol, Fluctuation-dissipation theorem in an isolated system of quantum dipolar Bosons after a quench, *Phys. Rev. Lett.* **111**, 050403 (2013), arXiv:1304.7279 [cond-mat.stat-mech].
- [25] A. Piñeiro Orioli and J. Berges, Breaking the fluctuation-dissipation relation by universal transport processes, *Phys. Rev. Lett.* **122**, 150401 (2019), arXiv:1810.12392 [cond-mat.quant-gas].
- [26] A. Schuckert and M. Knap, Probing eigenstate thermalization in quantum simulators via fluctuation-dissipation relations, *Phys. Rev. Research* **2**, 043315 (2020), arXiv:2007.10347 [cond-mat.quant-gas].
- [27] P. Hauke, M. Heyl, L. Tagliacozzo, and P. Zoller, Measuring multipartite entanglement through dynamic susceptibilities, *Nat. Phys.* **12**, 778 (2016), arXiv:1509.01739 [quant-ph].
- [28] R. Costa de Almeida and P. Hauke, From entanglement certification with quench dynamics to multipartite entanglement of interacting fermions, arXiv:2005.03049 [quant-ph] (2020).
- [29] C. L. Degen, F. Reinhard, and P. Cappellaro, Quantum sensing, *Rev. Mod. Phys.* **89**, 035002 (2017), arXiv:1611.02427 [quant-ph].
- [30] L. Pezzè, A. Smerzi, M. K. Oberthaler, R. Schmied, and P. Treutlein, Quantum metrology with nonclassical states

- of atomic ensembles, *Rev. Mod. Phys.* **90**, 035005 (2018), arXiv:1609.01609 [quant-ph].
- [31] T. S. Grigera and N. E. Israeloff, Observation of fluctuation-dissipation-theorem violations in a structural glass, *Phys. Rev. Lett.* **83**, 5038 (1999), arXiv:cond-mat/9904351 [cond-mat.dis-nn].
- [32] L. Bellon and S. Ciliberto, Experimental study of the fluctuation dissipation relation during an aging process, *Phys. D: Nonlinear Phenom.* **168-169**, 325 (2002), arXiv:cond-mat/0201224 [cond-mat.mtrl-sci].
- [33] R. R. Netz, Fluctuation-dissipation relation and stationary distribution of an exactly solvable many-particle model for active biomatter far from equilibrium, *J. Chem. Phys.* **148**, 185101 (2018), <https://doi.org/10.1063/1.5020654>.
- [34] J. von Neumann, *Mathematische Grundlagen der Quantenmechanik* (Springer, Berlin, 1932) [J. von Neumann, *Mathematical foundations of quantum mechanics*, translated by R. T. Beyer (Princeton University Press, Princeton, 1955)].
- [35] O. Romero-Isart, M. Rizzi, C. A. Muschik, E. S. Polzik, M. Lewenstein, and A. Sanpera, Quantum memory assisted probing of dynamical spin correlations, *Phys. Rev. Lett.* **108**, 065302 (2012), arXiv:1105.6308 [quant-ph].
- [36] M. Knap, A. Kantian, T. Giamarchi, I. Bloch, M. D. Lukin, and E. Demler, Probing real-space and time-resolved correlation functions with many-body Ramsey interferometry, *Phys. Rev. Lett.* **111**, 147205 (2013), arXiv:1307.0006 [cond-mat.quant-gas].
- [37] J. S. Pedernales, R. Di Candia, I. L. Egusquiza, J. Casanova, and E. Solano, Efficient quantum algorithm for computing n -time correlation functions, *Phys. Rev. Lett.* **113**, 020505 (2014), arXiv:1401.2430 [quant-ph].
- [38] P. Uhrich, S. Castrignano, H. Uys, and M. Kastner, Noninvasive measurement of dynamic correlation functions, *Phys. Rev. A* **96**, 022127 (2017), arXiv:1611.08123 [quant-ph].
- [39] M. Kastner and P. Uhrich, Reducing backaction when measuring temporal correlations in quantum systems, *Eur. Phys. J. ST* **227**, 365 (2018), arXiv:1710.00188 [quant-ph].
- [40] P. Uhrich, C. Gross, and M. Kastner, Probing unitary two-time correlations in a neutral atom quantum simulator, *Quantum Sci. Technol.* **4**, 024005 (2019), arXiv:1806.01758 [quant-ph].
- [41] A. Roggero and J. Carlson, Dynamic linear response quantum algorithm, *Phys. Rev. C* **100**, 034610 (2019), arXiv:1804.01505 [quant-ph].
- [42] D. Yang, A. Grankin, L. M. Sieberer, D. V. Vasilyev, and P. Zoller, Quantum non-demolition measurement of a many-body Hamiltonian, *Nat. Commun.* **11**, 775 (2020), arXiv:1905.06444 [quant-ph].
- [43] L. Pan, X. Chen, Y. Chen, and H. Zhai, Non-Hermitian linear response theory, *Nat. Phys.* **16**, 767 (2020), arXiv:1909.12516 [cond-mat.quant-gas].
- [44] D. Sticlet, B. Dóra, and C. Paşcu Moca, Kubo formula for non-Hermitian systems and tachyon optical conductivity, arXiv:2104.02428 [cond-mat.quant-gas] (2021).
- [45] A. M. Kaufman, M. E. Tai, A. Lukin, M. Rispoli, R. Schittko, P. M. Preiss, and M. Greiner, Quantum thermalization through entanglement in an isolated many-body system, *Science* **353**, 794 (2016), arXiv:1603.04409 [quant-ph].
- [46] R. El-Ganainy, K. G. Makris, M. Khajavikhan, Z. H. Musslimani, S. Rotter, and D. N. Christodoulides, Non-Hermitian physics and PT symmetry, *Nat. Phys.* **14**, 11 (2018).
- [47] Y. Ashida, Z. Gong, and M. Ueda, Non-Hermitian physics, arXiv:2006.01837 [cond-mat.mes-hall] (2020).
- [48] A. Guo, G. J. Salamo, D. Duchesne, R. Morandotti, M. Volatier-Ravat, V. Aimez, G. A. Siviloglou, and D. N. Christodoulides, Observation of \mathcal{PT} -symmetry breaking in complex optical potentials, *Phys. Rev. Lett.* **103**, 093902 (2009).
- [49] C. E. Rüter, K. G. Makris, R. El-Ganainy, D. N. Christodoulides, M. Segev, and D. Kip, Observation of parity-time symmetry in optics, *Nat. Phys.* **6**, 192 (2010).
- [50] M. Naghiloo, M. Abbasi, Y. N. Joglekar, and K. W. Murch, Quantum state tomography across the exceptional point in a single dissipative qubit, *Nat. Phys.* **15**, 1232 (2019), arXiv:1901.07968 [quant-ph].
- [51] W. Cao, X. Lu, X. Meng, J. Sun, H. Shen, and Y. Xiao, Reservoir-mediated quantum correlations in non-Hermitian optical system, *Phys. Rev. Lett.* **124**, 030401 (2020), arXiv:1903.12213 [quant-ph].
- [52] W. Chen, M. Abbasi, Y. N. Joglekar, and K. W. Murch, Quantum jumps in the non-Hermitian dynamics of a superconducting qubit, arXiv:2103.06274 [quant-ph] (2021).
- [53] F. E. Öztürk, T. Lappe, G. Hellmann, J. Schmitt, J. Klaers, F. Vewinger, J. Kroha, and M. Weitz, Observation of a non-Hermitian phase transition in an optical quantum gas, *Science* **372**, 88 (2021), arXiv:2010.15829 [cond-mat.quant-gas].
- [54] T. E. Lee, F. Reiter, and N. Moiseyev, Entanglement and spin squeezing in non-Hermitian phase transitions, *Phys. Rev. Lett.* **113**, 250401 (2014), arXiv:1409.7067 [cond-mat.quant-gas].
- [55] Y. Ashida, S. Furukawa, and M. Ueda, Parity-time-symmetric quantum critical phenomena, *Nat Commun* **8**, 15791 (2017), arXiv:1611.00396 [cond-mat.stat-mech].
- [56] S. Yao and Z. Wang, Edge states and topological invariants of non-Hermitian systems, *Phys. Rev. Lett.* **121**, 086803 (2018), arXiv:1803.01876 [cond-mat.mes-hall].
- [57] M. Nakagawa, N. Kawakami, and M. Ueda, Non-Hermitian Kondo effect in ultracold alkaline-earth atoms, *Phys. Rev. Lett.* **121**, 203001 (2018), arXiv:1806.04039 [cond-mat.quant-gas].
- [58] R. Hamazaki, K. Kawabata, and M. Ueda, Non-Hermitian many-body localization, *Phys. Rev. Lett.* **123**, 090603 (2019), arXiv:1811.11319 [cond-mat.dis-nn].
- [59] M. Nakagawa, N. Tsuji, N. Kawakami, and M. Ueda, Dynamical sign reversal of magnetic correlations in dissipative Hubbard models, *Phys. Rev. Lett.* **124**, 147203 (2020), arXiv:1904.00154 [cond-mat.quant-gas].
- [60] J. Wiersig, Review of exceptional point-based sensors, *Photon. Res.* **8**, 1457 (2020).
- [61] J. Wiersig, Prospects and fundamental limits in exceptional point-based sensing, *Nat. Commun.* **11**, 2454 (2020).
- [62] G. P. Berman and A. I. Nesterov, Non-Hermitian adiabatic quantum optimization, *Int. J. Quantum Inf.* **07**, 1469 (2009), arXiv:<https://doi.org/10.1142/S0219749909005961> [quant-ph].
- [63] A. I. Nesterov and G. P. Berman, Quantum search using non-Hermitian adiabatic evolution, *Phys. Rev. A* **86**, 052316 (2012), arXiv:1208.4642 [quant-ph].

- [64] B. Misra and E. C. G. Sudarshan, The Zeno's paradox in quantum theory, *Journal of Mathematical Physics* **18**, 756 (1977), <https://doi.org/10.1063/1.523304>.
- [65] P. Facchi and S. Pascazio, Quantum Zeno dynamics: mathematical and physical aspects, *J. Phys. A: Math. Theor.* **41**, 493001 (2008), arXiv:0903.3297 [math-ph].
- [66] K. Stannigel, P. Hauke, D. Marcos, M. Hafezi, S. Diehl, M. Dalmonte, and P. Zoller, Constrained dynamics via the Zeno effect in quantum simulation: Implementing non-Abelian lattice gauge theories with cold atoms, *Phys. Rev. Lett.* **112**, 120406 (2014), arXiv:1308.0528 [quant-ph].
- [67] F. Schäfer, T. Fukuhara, S. Sugawa, Y. Takasu, and Y. Takahashi, Tools for quantum simulation with ultracold atoms in optical lattices, *Nat. Rev. Phys.* **2**, 411 (2020), arXiv:2006.06120 [cond-mat.quant-gas].
- [68] B. Svensson, Pedagogical review of quantum measurement theory with an emphasis on weak measurements, *Quanta* **2**, 18 (2013).
- [69] J. Dalibard, Y. Castin, and K. Mølmer, Wave-function approach to dissipative processes in quantum optics, *Phys. Rev. Lett.* **68**, 580 (1992).
- [70] K. Mølmer, Y. Castin, and J. Dalibard, Monte Carlo wave-function method in quantum optics, *J. Opt. Soc. Am. B* **10**, 524 (1993).
- [71] A. J. Daley, Quantum trajectories and open many-body quantum systems, *Adv. Phys.* **63**, 77 (2014), arXiv:<https://doi.org/10.1080/00018732.2014.933502> [quant-ph].
- [72] G. Aarts and J. Berges, Nonequilibrium time evolution of the spectral function in quantum field theory, *Phys. Rev. D* **64**, 105010 (2001), arXiv:hep-ph/0103049 [hep-ph].
- [73] C. Gardiner and P. Zoller, *Quantum Noise: A Handbook of Markovian and Non-Markovian Quantum Stochastic Methods with Applications to Quantum Optics*, 3rd ed., Springer Series in Synergetics (Springer-Verlag Berlin Heidelberg, 2004).
- [74] H.-P. Breuer and F. Petruccione, *The Theory of Open Quantum Systems* (Oxford University Press, Oxford, 2007).
- [75] B. Militello and A. Napoli, Hilbert space partitioning for non-Hermitian Hamiltonians: From off-resonance to Zeno subspaces, *Phys. Lett. A* **384**, 126355 (2020), arXiv:1907.01969 [quant-ph].
- [76] A. Biella and M. Schiró, Many-body quantum Zeno effect and measurement-induced subradiance transition, arXiv:2011.11620 [quant-ph] (2020).
- [77] W. S. Bakr, J. I. Gillen, A. Peng, S. Fölling, and M. Greiner, A quantum gas microscope for detecting single atoms in a Hubbard-regime optical lattice, *Nature (London)* **462**, 74 (2009), arXiv:0908.0174 [cond-mat.quant-gas].
- [78] J. F. Sherson, C. Weitenberg, M. Endres, M. Cheneau, I. Bloch, and S. Kuhr, Single-atom-resolved fluorescence imaging of an atomic Mott insulator, *Nature (London)* **467**, 68 (2010), arXiv:1006.3799 [cond-mat.quant-gas].
- [79] C. Maier, T. Brydges, P. Jurcevic, N. Trautmann, C. Hempel, B. P. Lanyon, P. Hauke, R. Blatt, and C. F. Roos, Environment-assisted quantum transport in a 10-qubit network, *Phys. Rev. Lett.* **122**, 050501 (2019), arXiv:1809.07680 [quant-ph].
- [80] P. E. Kloeden and E. Platen, *Numerical Solution of Stochastic Differential Equations*, 1st ed., Stochastic Modelling and Applied Probability, Vol. 23 (Springer-Verlag Berlin Heidelberg, 1992).
- [81] C. Gardiner, *Stochastic Methods: A Handbook for the Natural and Social Sciences*, 4th ed., Springer Series in Synergetics, Vol. 13 (Springer-Verlag Berlin Heidelberg, 2009).
- [82] A. Barchielli and M. Gregoratti, *Quantum Trajectories and Measurements in Continuous Time: The Diffusive Case*, 1st ed., Lecture Notes in Physics, Vol. 782 (Springer-Verlag Berlin Heidelberg, 2009).
- [83] K. Jacobs and D. A. Steck, A straightforward introduction to continuous quantum measurement, *Contemporary Physics* **47**, 279 (2006), arXiv:quant-ph/0611067 [quant-ph].
- [84] H. M. Wiseman and G. J. Milburn, *Quantum Measurement and Control* (Cambridge University Press, 2009).
- [85] H. Hasegawa and H. Ezawa, Stochastic calculus and some models of irreversible processes, *Progress of Theoretical Physics Supplement* **69**, 41 (1980).
- [86] I. Semina, V. Semin, F. Petruccione, and A. Barchielli, Stochastic Schrödinger equations for Markovian and non-Markovian cases, *Open Sys. Inf. Dyn.* **21**, 1440008 (2014), arXiv:1310.0644 [quant-ph].
- [87] N. Gisin and I. C. Percival, The quantum-state diffusion model applied to open systems, *J. Phys. A: Math. Gen.* **25**, 5677 (1992).
- [88] K. Burrage and P. Burrage, High strong order methods for non-commutative stochastic ordinary differential equation systems and the Magnus formula, *Phys. D: Non-linear Phenom.* **133**, 34 (1999).
- [89] S. Blanes, F. Casas, J. Oteo, and J. Ros, The Magnus expansion and some of its applications, *Phys. Rep.* **470**, 151 (2009), arXiv:0810.5488 [math-ph].
- [90] K. Kamm, S. Pagliarani, and A. Pascucci, On the stochastic Magnus expansion and its application to SPDEs, arXiv:2001.01098 [math.PR] (2020).
- [91] G. Lüders, Über die Zustandsänderung durch den Meßprozeß, *Annalen der Physik* **443**, 322 (1950).